CAPITAL UNIVERSITY OF SCIENCE AND
TECHNOLOGY, ISLAMABAD


# Photovoltaic Power Forecast in an Energy Management System for a Hybrid Microgrid

by

Muhammad Qasim Rauf

A thesis submitted in partial fulfillment for the
degree of Master of Science

in the

Faculty of Engineering
Department of Electrical Engineering

2020

*Dedicated to my Teachers who enlightened me with their knowledge.*

*And*

*Dedicated to my Parents without whom this document would have never materialized.*

*To my loving wife, for supporting me every step of the way.*


# CERTIFICATE OF APPROVAL

## Photovoltaic Power Forecast in an Energy Management System for a Hybrid Microgrid

by

Muhammad Qasim Rauf

(MEE181002)

### THESIS EXAMINING COMMITTEE

| S. No. | Examiner | Name | Organization |
|---|---|---|---|
| (a) | External Examiner | Dr. Tahir Ejaz | Grafton College, Islamabad |
| (b) | Internal Examiner | Dr. Umer Amir Khan | CUST, Islamabad |
| (c) | Supervisor | Dr. Muhammad Ashraf | CUST, Islamabad |

Supervisor Name
Dr. Muhammad Ashraf
November, 2020

Dr. Noor Muhammad Khan
Head
Dept. of Electrical Engineering
November, 2020

Dr. Imtiaz Ahmad Taj
Dean
Faculty of Engineering
November, 2020

# *Author's Declaration*

I, **Muhammad Qasim Rauf** hereby state that my MS thesis titled "**Photovoltaic Power Forecast in an Energy Management System for a Hybrid Microgrid**" is my own work and has not been submitted previously by me for taking any degree from Capital University of Science and Technology, Islamabad or anywhere else in the country/abroad.

At any time if my statement is found to be incorrect even after my graduation, the University has the right to withdraw my MS Degree.

**(Muhammad Qasim Rauf)**
Registration No: MEE181002

# *Plagiarism Undertaking*

I solemnly declare that research work presented in this thesis titled "**Photovoltaic Power Forecast in an Energy Management System for a Hybrid Microgrid** " is solely my research work with no significant contribution from any other person. Small contribution/help wherever taken has been dully acknowledged and that complete thesis has been written by me.

I understand the zero tolerance policy of the HEC and Capital University of Science and Technology towards plagiarism. Therefore, I as an author of the above titled thesis declare that no portion of my thesis has been plagiarized and any material used as reference is properly referred/cited.

I undertake that if I am found guilty of any formal plagiarism in the above titled thesis even after award of MS Degree, the University reserves the right to withdraw/revoke my MS degree and that HEC and the University have the right to publish my name on the HEC/University website on which names of students are placed who submitted plagiarized work.

**(Muhammad Qasim Rauf)**
Registration No: MEE181002

# *Acknowledgements*

In the name of Allah SWT The Most Beneficent and The Most Merciful. All praises are to Allah SWT for all blesses so that the writer can accomplish this thesis. In addition, may peace and salutation be given to the prophet Muhammad (pbuh) who has taken all human being from the darkness to the lightness.

I would like to express my heartiest gratitude to my supervisor Prof. Dr.Muhammad Ashraf, Electrical Dept, Capital University of Science and Technology (CUST), for his efforts to establish research environments and activities at CUST. It was a wonderful experience and learning opportunity to work with him as a MS student. I am really indebted to his kind support and all out help to complete this research work successfully. His continuous encouragement, support and constructive criticism made me able to complete this task. In spite of his engagements, his dedication, as a supervisor, is highly appreciable.

I feel honor to express my feeling of appreciation for the support I have received from my colleges especially abc, acd and cde who helped me in my research work and documentation of the thesis.

**(Muhammad Qasim Rauf)**

Registration No: MEE181002

# *Abstract*

Unpredictable nature of renewable energy (RE) sources like solar and wind challenges grid utilities to reliably match power supply and demand, across centralized grid networks. As a result, forecasting techniques have gained tremendous importance among grid operators in order to economically integrate Photovoltaic (PV) power sources. This thesis rendition aims at developing an Energy Management Scheme (EMS) with an accurate forecasting mechanism at the helm, to dispatch a sample hybrid microgrid. Machine Learning (ML) based forecasting is an effective tool used to estimate maximum power output from a solar generator against any given climate conditions. In this study, a deterministic (DTRM) model for a 100kW PV generator is developed using standard 5-parameter solar cell model. In this study a number of ML models like Gaussian Process Regression with Rational Quadratic (RQGPR) kernel, Gaussian Process Regression with Matern 5/2 kernel (M5/2GPR), and Linear Support Vector Machine (LSVM) are trained using climate dataset acquired from a weather station installed at Islamabad, Pakistan. Qualitative analysis of said algorithms is done using Root Mean Squared Error (RMSE) as Key Performance Indicator (KPI). It is concluded that RQGPR returned lowest RMSE value while DTRM returned fastest training time, and vice versa. After DTRM, LSVM returned the highest RMSE level, followed by M5/2GPR. EMS aided by RQGPR forecast engine is tasked with keeping grid power balance and sufficient battery storage level, during uncertain climate conditions. EMS performs the said task by appropriately dispatching energy sources in a sample microgrid. Grid power balance is represented by the deviation of grid frequency from nominal value of 50Hz. A number of microgrid variables are observed and presented.

# Contents

# List of Figures

# List of Tables

# Abbreviations

| | |
|---|---|
| **AI** | Artificial Intelligence |
| **ANN** | Artificial Neural Network |
| **ARIMA** | Autoregressive Integrated Moving Average Model |
| **BSS** | Battery Storage System |
| **EMS** | Energy Management System |
| **GHI** | Global Horizontal Irradiance |
| **GPR** | Gaussian Process Regression |
| **IC** | Incremental Conductance |
| **IEC** | International Energy Commission |
| **LSTM** | Long Short-Term Memory |
| **LSVM** | Linear Support Vector Machine |
| **M5/2GPR** | Matern 5/2 Gaussian Process Regression |
| **MAPE** | Mean Absolute Percentage Error |
| **ML** | Machine Learning |
| **MPP** | Maximum Power Point |
| **MPPT** | Maximum Power Point Tracking |
| **MV** | Medium Voltage |
| **NREL** | National Renewable Energy Laboratory |
| **P&O** | Perturb and Observe |
| **PCC** | Point of Common Coupling |
| **PID** | Proportional Integral Derivative |
| **POP** | Point of Operation |
| **PU** | Per Unit |
| **PV** | Photovoltaic |

| | |
|---|---|
| **PVG** | Photovoltaic Generator |
| **PWM** | Pulse Width Modulation |
| **RMSE** | Root Mean Squared Error |
| **RQGPR** | Rational Quadratic Gaussian Process Regression |
| **STC** | Standard Test Conditions |
| **SVM** | Support Vector Machine |
| **USAID** | United States Agency for International Development |

# Symbols

| | |
|---|---|
| $V_{OC}$ | Open circuit voltage of a PV generator |
| $I_{SC}$ | Short circuit current of a PV generator |
| $P_{m,h}$ | Average measured power |
| $P_{p,h}$ | Predicted power |
| $e_h$ | Prediction error |
| $V_D$ | Forward diode voltage |
| $R_{Sh}$ | Shunt resistance of a PV generator |
| $R_{Ser}$ | Series resistance of a PV generator |
| $\epsilon_g$ | Band gap energy of photodiode |
| $P_{Det}$ | Estimated power from Deterministic technique |
| $P_{Out}$ | Total power output from microgrid |
| $f_g$ | Grid frequency |

# Chapter 1

# Introduction

## 1.1 Introduction

PV power forecasting has become a cornerstone of energy management schemes in order to securely and economically integrate a PVG into the smart grid.
This study presents the importance of an accurate forecast model of a Photovoltaic Generator (PVG) and integrates the forecasting model in an Energy Management Scheme (EMS) developed for a hybrid microgrid. The main purpose of this thesis is to compare various PVG modeling techniques in terms of performance metrics and embed the most accurate model in an EMS. The EMS response is observed and presented for a microgrid which is exposed to multiple grid contingency events like islanding and supplementary loading events.
A mandatory requirement for a stable power grid operation is to balance the differences between power supply and demand. Grid operators are responsible for scheduling power reserves and they must be aware of future or upcoming values of electric-load as well as supply. However, the problem is compounded for Renewable Energy Sources (RES), in which case the output power depends on chaotic nature of climate conditions. RES power producers typically use short-term power forecasts to prepare sale offers (bids) for electricity market. RES power producers are heavily penalized if they fail to follow scheduled bid. Therefore, in order to

boost profits and reduce penalties, an accurate forecast mechanism is extremely important for RES power production.
Smart grid requirement entails a multi-agent architecture for microgrid operation. Distributed Generators (DGs) like PVGs, wind turbines, Battery Storage System (BSS) are considered microgrid agents. An EMS enforces a coherent strategy that eventually develops cooperation between these agents. EMS also guarantees grid's operational reliability by undertaking uncertainties of renewable generation, demand and market prices. Short-term forecasting engines are embedded in an EMS to reduce forecast errors. In the first stage forecasting engines produce estimates on uncertain grid parameters. In the second stage the EMS takes actions based on those estimates. In this case the forecast accuracy has a direct impact on EMS response; any imprecise prediction can produce devastating impact on the grid e.g., undue maintenance, blackouts etc.

In essence, this thesis rendition models a forecasting engine for a 100kW PVG in MATLAB. Physical or deterministic, and probabilistic modeling techniques are used to approximate the PVG response towards changing climate conditions. Deterministic modeling is based on PV parameters outlined in a manufacturer's datasheet, and the elementary physics that defines PVG response. Probabilistic techniques are based on Machine Learning (ML) paradigm, and a number of mainstream algorithms like Matern 5/2 Gaussian Process Regression ($M5/2GPR$), Rational Quadratic Gaussian Process Regression (RQGPR), and Support Vector Machine (SVM) are used. The performance of all these techniques are compared in terms of key performance metrics like Root Mean Squared Error or RMSE. The most accurate technique or the one with the lowest RMSE is chosen and integrated in a Weighted Energy Scheduling Scheme (WESS). The importance of an accurate forecast is validated by observing the WESS response during emergency events in a hybrid microgrid.

It is concluded from the study that the proposed EMS with an accurate forecasting technique has performed satisfactorily under several conditions. Further

future work is also recommended in the concluding chapter.

## 1.2 Background and Motivation

In the context of modern energy an ever-growing energy demand requires assurances on grid safety and reliability, minimum differences between power supply and demand, and integration of RE. Secure power generation, transmission and distribution is extremely vulnerable due to several environmental, technical and economic constraints. A power fluctuation of even a few minutes can potentially set in motion a domino effect, resulting in conventional production units grinding to a halt. The number of conventional production units are constantly required to grow to mitigate supply-demand differences. RES based production units are an invaluable alternative to more expensive nuclear, hydel or gas-turbine based power producers. The input requirements of RES are extremely low. The low-carbon footprint is an added benefit of RES power generation. Power fluctuations can be greatly minimized by better RES integration in power grid, complemented by demand response i.e., change electrical loads in response to changes in supply.
The concept of smart grid is based on a delivery mechanism that efficiently produces, transports and distributes the power from producers to consumers. Smart grid heavily relies on modern communication and information technology infrastructure. However, the simplest goal of a smart grid is to balance electricity generation and consumption using sensors, monitoring, analysis and communications. In this context, microgrid is used for decentralized energy production with an ability to operate both grid-connected and off-grid. In grid-connected mode, the microgrid can either provide or receive power from the utility grid. However, during off-grid (or islanding) period, the microgrid must seamlessly supply power to its local load. Generally, a microgrid is expected to observe power demand and control power generators accordingly, provide ancillary services and inject power into the utility grid if and when required.
PV power forecasting has become a cornerstone of energy management schemes in order to securely and economically integrate a PVG into the smart grid. Ancillary

costs associated with volatile PV power output can significantly be reduced due to an accurate forecast. Grid operations like real-time power grid dispatch, storage control, and electricity market clearing hugely benefit from ultra-short term forecasts [1], e.g., Australian market uses forecast resolution of 5-minutes as reported in [2]. Short-term PV power forecasts (e.g., 24hours ahead) is also an important tool for solar power traders. Forecasts can greatly enhance delivered power quality. However, due to chaotic nature of climate conditions the accuracy of a PV model can deteriorate. Model precision is compromised in the presence of atmospheric conditions like temperature, cloud index, relative humidity etc.

The motivation of this work is to develop an EMS based on a prediction algorithm for PVG power production. The robustness of EMS is evaluated against microgrid contingency events e.g., unpredictable climate conditions, supplementary loading and islanding events. The objective is to design and analyze an efficient EMS that effectively dispatches power across a hybrid microgrid.

## 1.3 Construction of a Photovoltaic Generator

A Photovoltaic Generator is predominantly made of photovoltaic (PV) solar cells. Other system components include batteries, charge controller, inverter etc. A single PV cell can generate about 1 or 2 W of power approximately, which also depends on the type of material used in PV cell construction [3]. PV cells are connected together in specific configuration to achieve bigger modules with higher power capacity. The maximum power capacity of a PV-module is not greater than 1kW. Modules can be grouped together to form PV-arrays – a crucial element in a PVG based power plant.

According to the available statistics, global PV market is steadily growing at a 30 percent per annum. Reason behind this growth is attributed to reliable power production without any fuel consumption, and the ability to deploy a PV power house virtually at any place where the sun shines. Modular technology enables to configure a PV system for varying power capacities, ranging from watts to megawatts.

One of the most disruptive factors in PV cell design is the limited efficiency of a solar cell. Typically, a solar cell can offer an efficiency of 18.3 percent only, depending on the construction technology. Current research indicates that all the PV materials have physical limits on the electricity they can produce. For instance, the maximum efficiency of crystalline Silicon is merely 28 percent.
Reliability of a PVG is a crucial factor and with a fault-tolerant circuit design the impact of component failure on overall system can be minimized. A number of redundant features are included in a PVG to protect module yield and restrict power degradation. Due to partial shading issues, a PVG is protected from potential hotspots by using bypass diodes across each solar cell. Typically, a PV module consists of one bypass diode per 18 solar cells [3].
As stated earlier, almost always a stand-alone solar cell is not powerful enough to produce required voltages and currents. Thereby a PV generator is shipped in the form of a parallel/series circuit configuration of solar cells. Multiple solar cells makeup a PV-module, multiple modules are assembled to form strings, multiple strings are joined to form a PV array/generator, as shown in Fig (1.1).
For example, a PVG of 66-strings of 5-series connected modules ($305W/module$) would yield a net power of 66x5x305=100 kW.

### 1.3.1 PV Module Performance Parameters

The following parameters are also used to qualify a PV module:

- **Peak-Watt or Maximum Power Point (MPP):** determined by measuring the maximum power output of a PV module under laboratory Standard Test Conditions (STC) i.e., 1000 W/$m^2$ and 25$^o$C.
- **Power Output Power Output:** represented in Watts and it is the power available at the input of the charge controller or regulator.
- **Energy Output:** indicates the amount of energy produced by the module during certain timer period, and represented in Watt-hour/$m^2$.

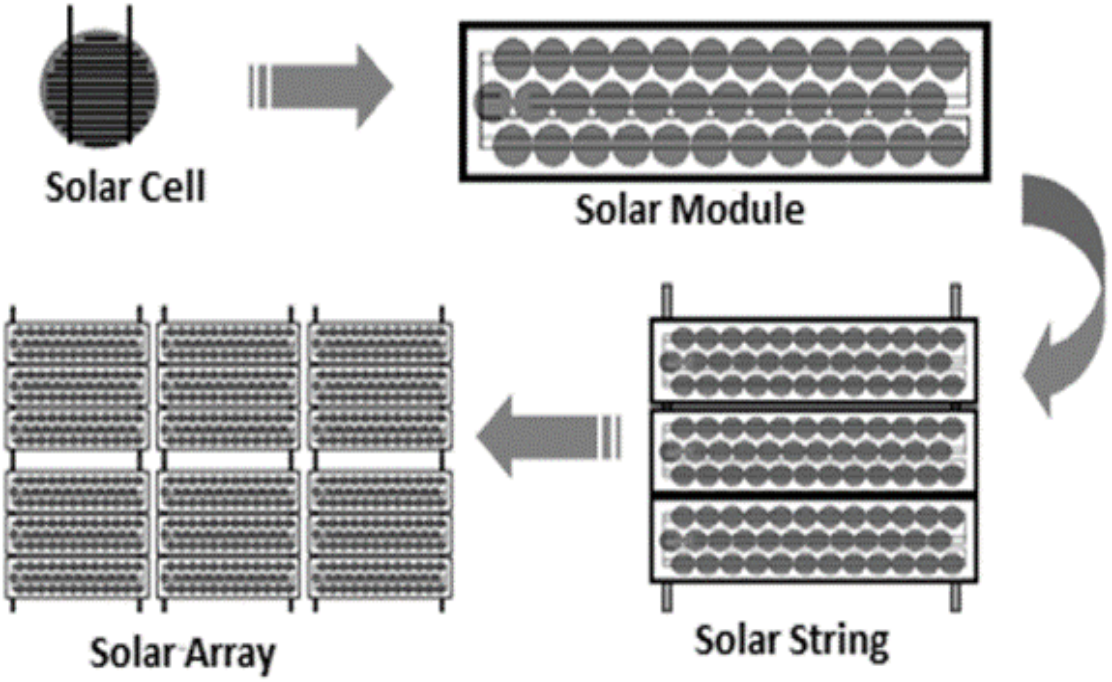


FIGURE 1.1: Solar Cell Configurations [4]

- **Conversion Efficiency:** is the ratio of energy delivered as output divided by the energy input from the sun.

## 1.4 Photovoltaic Characteristics

Typical PV characteristics are shown in 1.2. As evident from the V-I curve, the voltage and current of a solar cell do not exhibit a linear relationship. Additionally, the P-V curve of the solar cell is non-monotonic. There are three important things to note about this curve,

1. Open Circuit Voltage ($V_{OC}$)–PV voltage for $\infty$ load resistance.
2. Short Circuit Current ($I_{SC}$)–PV current for zero load resistance.
3. Maximum Power Point (MPP).

The non-monotonicity of graphs in Fig (1.2) is due to the following factors:

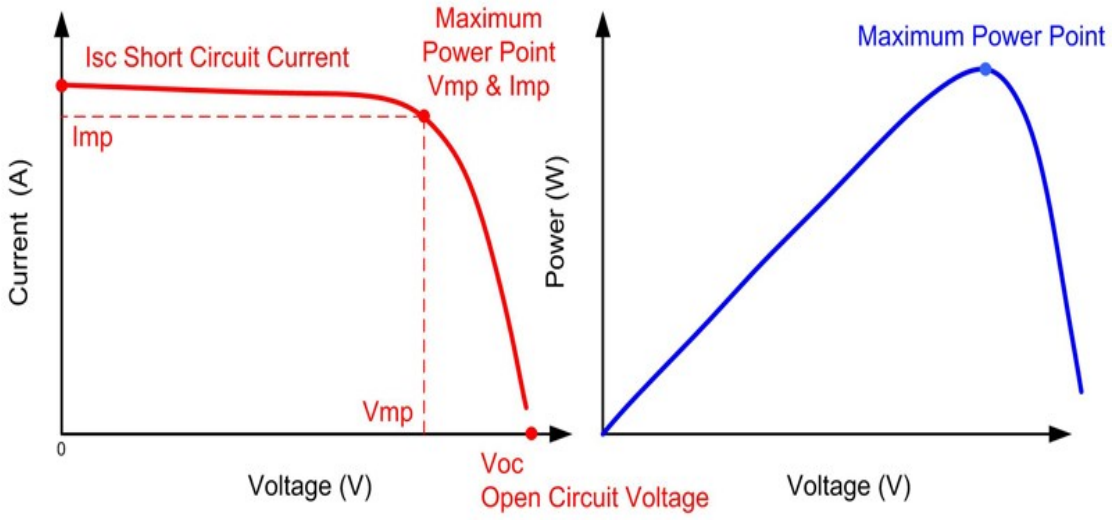


FIGURE 1.2: PV Characteristics (P-V, and V-I) of a Typical Solar Cell [5]

.

- Solar Irradiation
- Operational temperature
- Load

The peak of the P-V curve (or the knee of the V-I curve) is known as the Maximum Power Point (MPP) of operation, and this is where all the above factors are optimized to yield maximum PV efficiency.

## 1.5 Maximum Power Point Tracking

An optimum load choice is crucial for maximum efficiency extraction from a solar cell. To fulfill this optimum load requirement modern power electronic converters are equipped with Maximum Power Point Tracking (MPPT) operation [6]. Their purpose is to sample the power output of PV-cell, analyze it and apply an optimal load value to gain maximum power for a given set of ecological conditions [7]. By controlling the amount of voltage from the PV-cell, the MPPT controllers achieve this objective.

MPPT is not to be confused with the mechanical tracking mechanism of solar

cells. MPPT is purely an electronic control system that tries to extract all the instantaneous power a solar cell can generate. Several MPPT algorithms can perform this task:

- Perturb and Observe (PO) Method.
- Incremental Conductance (IC) Method.
- Fractional Open-Circuit Voltage Method.
- Fractional Short-Circuit Current Method.
- Current Sweep Method.
- DC-Link Capacitor Droop Control Method.

The energy management scheme used in Chapter 4 provides power output from its solar panels using the IC method. Therefore, the following section only discusses the said method. Rest of the methods are beyond the scope of this thesis work.

### 1.5.1 Incremental Conductance (IC) Method

This method involves a continuous sampling of output voltage and current of the PV-system. The output voltage is adjusted based on the incremental and instantaneous conductance of the PV-system. The entire region of solar panel operation is divided into two categories as indicated in 1.3 region-1 where $dP/dV > 0$, and region-2 where $dP/dV < 0$. The POP where $dP/dV = 0$ represents the MPP. Substituting $P = VI$ and solving the differential equation by chain rule gives control law as depicted in equation 1.1 for MPPT controller,

$$\begin{aligned} &\frac{d}{dV}IV = 0 \\ &I\frac{dV}{dV} + V\frac{dI}{dV} = 0 \\ &I + V\frac{dI}{dV} = 0 \\ &\frac{dI}{dV} = -\frac{I}{V} \end{aligned} \tag{1.1}$$

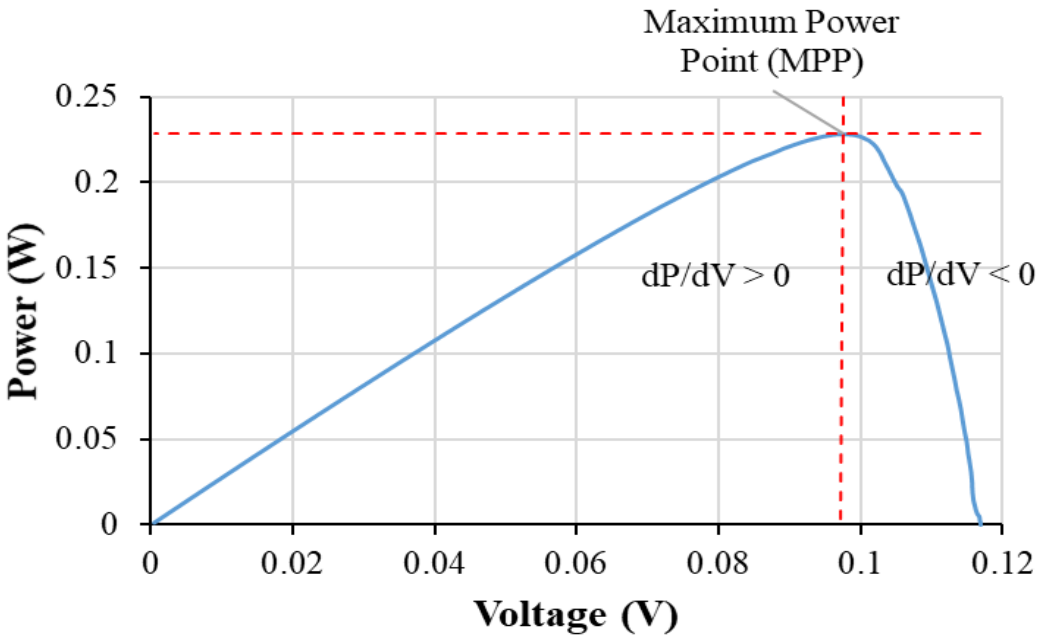


FIGURE 1.3: Regions of Operation for Incremental Conductance Technique.

The IC algorithm implements control law in eq (1.1) according to the flowchart in Fig (1.4).

## 1.6 Machine Learning

Machine learning is a branch of Artificial Intelligence (AI) and it empowers systems to automatically learn and improve from experience without the need of an explicit software update. Machine learning is essentially concentrated on computer programs that access historical data to learn. Real-world data is usually incomplete, or the data is collated in a variety of formats e.g., a real-world problem might use different data types like sensor signals, text and images from camera etc.

Learning begins with observations and meaningful data collection, either automatically or manually. A computer powered by machine learning looks for patterns in the data and makes better decisions in the future based on the past observations. Primary aim of the entire practice is to make computers smart enough to learn

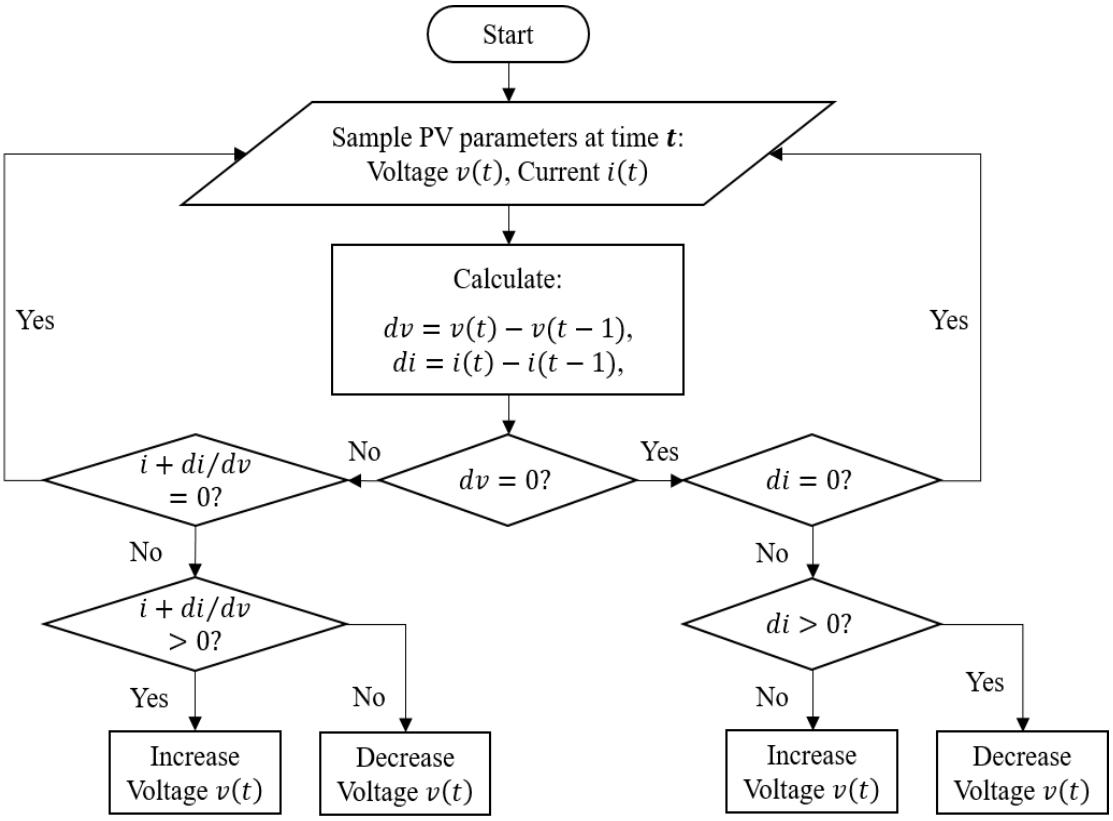


FIGURE 1.4: Flow Chart Description of Incremental Conductance Technique.

automatically without human intervention [8]. Machine learning algorithms typically build a mathematical model based on historical observations called "training data" [9] [10].

Choosing the right machine learning model is all about trade-offs. A highly flexible model might over-fit a data by including minor details like noise into final model. On the other hand, a simple model might ignore vital modeling details. Additionally, a designer is frequently confronted with tradeoffs between model training speed, prediction accuracy and complexity level. A systematic workflow is mandatory to choose an appropriate machine-learning algorithm [11].

## 1.7 Types of Machine Learning Algorithms

Machine learning algorithms are broadly classified into two categories as shown in Fig 1.5.

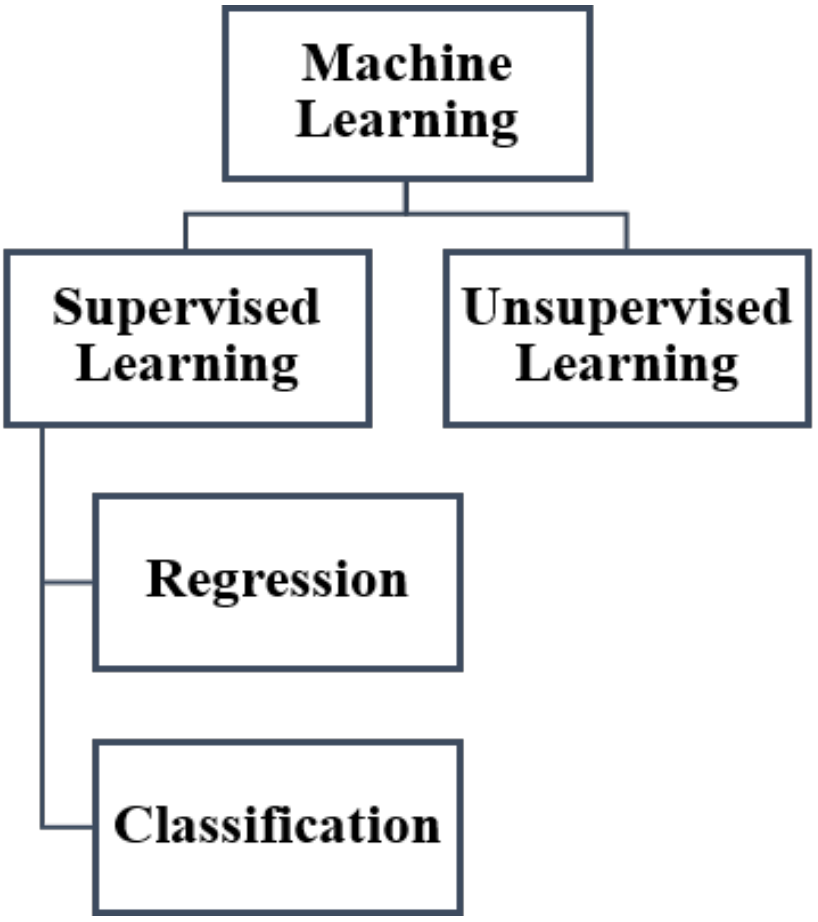


FIGURE 1.5: Machine Learning Algorithms Classification.

- Supervised Learning
- Unsupervised Learning

Supervised learning trains a model based on known input/s and predicts future outputs accordingly. The outcome of supervised learning is a model that makes predictions in the presence of uncertainty. Supervised learning techniques are further divided into classification and regression techniques.

Unsupervised learning detects intrinsic patterns in input training data. Unsupervised learning is useful in a situation when the user is uncertain what information the data contains, or when the data is without labeled responses. Clustering is an unsupervised learning technique used to find hidden patterns or groupings in a data. Major applications of clustering are market research, gene sequence analysis and object recognition [11]. Classification techniques provide prediction response based on categorical input data. Examples of classification would be a distinction

required to be made between a genuine email or a spam, or whether a tumor is benign or cancerous. Other typical applications of classification are in the fields of image and speech recognition and credit scoring.

## 1.8 Types of PV Power Forecast

Most of the PV power forecast techniques are designed to address a particular scenario with an emphasis on improvement of forecast quality. A number of modeling techniques can be used to forecast a PV power output. These techniques can be categorized into three approaches [1, 12, 13].

- Deterministic or physical modeling.
- Statistical or probabilistic or stochastic modeling.
- Hybrid modeling.

Deterministic approach focuses on modeling non-linear PVG power output due to ambient climate conditions. The primary advantage of deterministic technique is virtually little need for historical operational details of the PVG. However, reliability of deterministic forecasts is based on model's historical performance and therefore real-time forecast is less accurate and can lead to blackouts [14]. Deterministic forecasts are typically made by physics-based models that overtly make assumptions and simplifications, and are therefore have limited practical utility [15]. Techniques like Numerical Weather Prediction (NWP) are based on internal dynamics of a system and it is a deterministic technique [16]. Nevertheless, variable weather conditions render NWP ineffective and imprecise [14].
Statistical or probabilistic or stochastic modeling approach enables machine learning techniques. Machine learning is a significant power forecasting tool with training capability empowered by historical data. The mixture of two or more statistical techniques with deterministic approaches is called hybrid modeling.

PV output power forecasting techniques can also be categorized based on prediction time-horizon or the specific time-scale.
The forecasting techniques are categorized in terms of prediction time-horizons as following [17].

- Long- or medium-term forecast (days or weeks ahead).
- Short-term forecast (24 hours or a few hours ahead).
- Ultra-short-term forecast (seconds or a few minutes ahead) [1].

Another PV output power forecasting categorization can be made based on the type of input predictor or feature i.e.

- Direct prediction (training data is in time-series format e.g., Auto-Regressive and Moving Average (ARMA) model).
- Indirect prediction (training data can be from wide variety of data-types e.g., solar irradiance, temperature etc.) [18].

## 1.9 Key Performance Metrics

The performance comparison of ML models is complicated by a number of factors like unpredictable weather conditions at different locations, variation in prediction time-horizon (e.g., ultrashort or short) etc. Measurement precision is expected to greatly hamper the prediction error performance. In this work, a few common error indices are selected as model performance parameters [19]. Forecast error is formulated using eq (1.2)

$$e_h = P_{m,h} - P_{p,h} \tag{1.2}$$

Here $P_{m,h}$ is the average measured power and $P_{p,h}$ represents forecasted power as provided by a particular forecasting technique. The Mean Biased Error (MBE)

and Mean Absolute Error (MAE) are presented in eq (1.3) and eq (1.4) Linear cost function applications use MAE as an important performance metric.

$$MBE = \frac{1}{N}\sum_{i=1}^{N}(P_{m,h} - P_{p,h}) \tag{1.3}$$

$$MAE = \frac{1}{N}\sum_{i=1}^{N}|P_{m,h} - P_{p,h}| \tag{1.4}$$

Root Mean Squared Error (RMSE) is presented in eq (1.5). Here, N is total number of samples in the data space. The only disadvantage of RMSE is due to its inherent sensitivity to large prediction errors. Normalized RMSE is expressed as percentage of mean value.

$$RMSE = \sqrt{\frac{1}{N}\sum_{i=1}^{N}e_i^2} \tag{1.5}$$

The formula for Mean Absolute Percentage Error (MAPE) is illustrated in eq. 1.6. However, for $P_(m,h) = 0$ this index is undefined.

$$MAPE = \frac{1}{N}\sum_{i=1}^{N}e_i^2|\frac{P_{m,h} - P_{p,h}}{P_{m,h}}| \times 100 \tag{1.6}$$

Correlation of the above-mentioned error indices is discussed in [19]. In this thesis rendition, RMSE is opted as the key performance index (KPI) for forecast evaluation.

## 1.10 Thesis Outline

The rest of the thesis is divided into following chapters:

*Chapter 2:* discusses the work conducted on forecasting of PVG power production in the context of a weighted energy scheduling scheme for effective power grid dispatch. The chapter also identifies the gap and formulates the problem statement. Later, proposed methodology for the research work is presented.

*Chapter 3:* outlines the modeling of a 100kW photovoltaic array using physical or deterministic, and probabilistic or statistical forecast techniques. A benchmark for model performance is also presented using elementary load line analysis of the same PV array, in Simulink. A machine learning workflow is used to declare the most suitable statistical technique, to be integrated in an EMS discussed in Chapter 4.

*Chapter 4:* presents a weighted energy scheduling scheme or energy management scheme for a number of hybrid microgrid contingency events such as unpredictable climate conditions, supplementary loading and islanding events. The most suitable PV power forecasting technique from Chapter 3 is also integrated in the scheduling scheme. Critical grid parameters like voltage and frequency are monitored and examined as per the International Electrotechnical Commission (IEC) guidelines.

*Chapter 5:* gives the conclusions drawn from the study work. Later the recommended future work is also outlined in the end.

## 1.11 Summary

This introductory chapter presented the motivation of the research work presented in this thesis rendition. This chapter also presented a number of background concepts that are central to the research methodology presented in the next chapter.

# Chapter 2

# Literature Review

## 2.1 Literature Review

The development of Distributed Generators (DGs) based on Renewable Energy (RE) technologies is expected to liberalize electricity market and reduce global warming [20]. The active power output of PVG based DGs immensely fluctuate due to climate variations. The solar irradiance received on the Earth's surface is non-uniform, non-stationary and periodic (24-hours) in nature, due to Earth's continuous rotation and revolution. Therefore, output power of a PVG plant also exhibits non-stationary and periodic characteristic i.e., PVG power rises before noon and declines afternoon. Conventional PV power prediction methods cannot guarantee precise forecast without compensating for the non-stationary features of PVG output power [21].

The addition of a PVG based DG into the utility grid is therefore expected to significantly impede grid operation reliability. RE integrated microgrids are extremely vulnerable, since their operation is hugely dependent on meteorological conditions [15]. Economic and reliable system operation, supported by accurate statistical power forecast models is an important solution for PVG output volatility [22]. Precise internal active power reserve estimation of a Photovoltaic Generator (PVG) is

extremely important to combat multiple smart grid issues e.g., balance demand-supply differences, scheduling of generation, proactive power trading [23, 24]. An accurate PVG power forecast model enables optimum power dispatch [25], cost efficiency, and reliable power source [26] with reduced grid power imbalance events. Moreover, accurate forecast models facilitate Demand Side Management (DSM) with efficient load consumption schedules. Accurate forecast models offer utilities to effectively dispatch power [12, 23, 27, 28]. Electricity traders are more often interested in one-day ahead PV power production prediction [29]. Modern computer modeling has enabled methods and techniques for PV power forecast research [14, 30]. Forecasting algorithms are divided into three categories i.e., deterministic, probabilistic, and hybrid [1, 12, 13]. Deterministic technique models non-linear PVG output power due to ambient climate conditions. The primary advantage of deterministic technique is virtually little need for historical operational details of the PVG. However, reliability of deterministic forecasts is based on model's historical performance and therefore real-time forecast is less accurate and can lead to blackouts [14]. Deterministic forecasts are typically made by physics-based models that overtly make assumptions and simplifications, and are therefore have limited practical utility [15]. Techniques like Numerical Weather Prediction (NWP) are based on internal dynamics of a system and it is a deterministic technique [16]. Nevertheless, variable weather conditions render NWP ineffective and imprecise [14]. On the other hand, statistical approach enables machine learning techniques. Machine learning is a significant power forecasting tool with training capability empowered by historical data. The mixture of two or more stochastic techniques with deterministic approaches is called hybrid modeling. The purpose of any modeling technique is to overcome a particular set of shortcomings with an overall improvement in forecast accuracy. In terms of prediction time horizons or the specific time-scale, the PVG power forecast techniques are divided into three types: Long or medium term forecast (days or weeks ahead), short term forecast (one-day ahead or a few hours ahead), and ultra-short term forecast (seconds or a few minutes ahead) [17]. Real-time power grid dispatch, storage control, and electricity market clearing hugely benefit from ultra-short term forecasts [1], e.g.,

Australian market uses forecast resolution of 5-minutes as reported in [2]. An Extreme Learning Machine (ELM) is developed in [31] that accepts ambient temperature and Global Horizontal Irradiance (GHI) values and provides a 24h-ahead PVG power forecast. The results of ELM in [31] are benchmarked with a Back Propagation Artificial Neural Network (BP-ANN). In terms of input variables, the PVG power prediction techniques are classified into direct prediction, and indirect prediction [18]. The historical data used in direct prediction techniques is typically based on time-series format. Examples of direct prediction techniques are Auto-Regressive and Moving Average Model (ARMA) and Autoregressive Integrated Moving Average Model (ARIMA). On the other hand, indirect prediction takes into account wider input data types e.g., solar irradiance, temperature, humidity as furnished by NWP systems. Since PV power is more closely dependent on meteorological factors, therefore indirect methods are considered more accurate [18]. Nonlinear system approximation based on Artificial Neural Networks (ANN) and Support Vector Machine (SVM) methods offer accurate forecast [32]. ANN and SVM provide similar PVG power prediction accuracy; albeit SVM requires fewer historical samples and are harder to train. On the other hand, ANN requires a larger dataset to match SVM's prediction accuracy, and their training time increases significantly with increasing complexity of neural networks [18]. Comparison of deterministic and stochastic forecasts of a PVG day-ahead power output is done in [33]. An uncertainty analysis technique is developed for an urban microgrid with high PVG penetration [34]. First-in-first-out robust smoothing is merged with a double grid search SVM algorithm for prediction of power [35]. Gaussian weighted regression algorithm is developed in [14] to predict short-term PVG power output and the results are compared with multiple statistical techniques in terms of key performance metrics. A joint technique based on SVM and K-Nearest Neighbor algorithms is used in [36] for PVG power prediction. Three different neural networks for PVG power prediction are optimized in [37] using genetic algorithm. In [38] an adaptive neuro-fuzzy inference system (ANFIS) and ANN predict PV ground source heat pump mechanism performance. Ensemble forecasting is a major forecast algorithm used to predict PVG power output,

which uses historical observations and NWP to provide a set of power predictions. However, conventional ensemble prediction requires multiple simulations in similar time-frames and locations [39]. Model selection is a crucial design element for ensemble forecasting; no universally accepted model best describes any given situation [14]. A multiple-model framework is proposed in [40] to obtain better prediction accuracy. Ensemble forecasts contain subsets of all possible boundary conditions, initial conditions, and model classes, all of which makes this method computationally expensive [41]. One of the greatest challenges with introducing PVGs in a power grid is to utilize its maximum benefits without losing grid's operational reliability. PVG with Sodium-Sulphur (NaS) based Battery Storage System (BSS) is an economically viable option [42]. Energy scheduling schemes like state of charge and load-pattern comparison extensively use analytical modeling techniques [43, 44]. Without appropriate energy management in place, grid voltage or frequency stability is compromised. If the PVG power output is greater than the local demand at the Point of Common Coupling (PCC) then the excess power from Voltage Source Converters (VSC) produce reverse power flow, creating voltage rise in the feeder [45, 46]. High quality power flow for a hybrid microgrid consisted of battery storage, PV converter, and wind turbine is ensured in [47] using model predictive control based Energy Management System (EMS). The EMS is designed for a 3.5 MW system and simulated under variable energy supply and demand scenarios. An energy management scheme in [43] charges/discharges storage devices integrated with rooftop PVGs by matching the PV power output and load profile. The strategy is based upon charging/discharging rates of the storage devices. The study in [48] solves worst-case EMS/microgrid scenario as generated from Taguchi's orthogonal array testing. Optimal power flow problem is addressed in [49] using Mixed Integer Linear Programming (MILP). Storage dispatch during peak load hours is addressed in [35] by introducing weighted energy scheduling scheme. A distributed EMS is robustly modeled in [50] formulates multiple operational costs observed in hybrid microgrids. The robust EMS in [50] decomposes original power dispatch problem into smaller sub-problems and delegates those sub-problems to local controllers. A multi-agent microgrid energy management

scheme is presented in [51] for a day-ahead load dispatch, based on deep neural networks with conventional generators, wind-turbines, PVGs and BSS serving as agents. The paper in [52] presents a cooperative energy management strategy that addresses outstanding issues like grid Time-of-Use (TOU) tariffs, storage capacity, load and PVG power shedding etc.

## 2.2 Gap Analysis and Problem Statement

A PV based hybrid microgrid is expected to operate round the clock under the guidelines of a dispatch schedule negotiated in the electricity market. Additionally, the dispatch schedule should be flexible enough to accommodate ancillary services like grid-frequency and grid-voltage regulation. Both of these requirements entail an energy management scheme supplemented by an accurate short-term PV forecast (few seconds to a minute). The PV power output is significantly dependent on the chaotic climate conditions as stated in section 1.2. Therefore, forecast quality analysis of PV power output for multiple climate conditions is of paramount importance. To the best of the author's understanding none of the studies in 2.1 undertook algorithm prediction quality analysis for different weather conditions. Performance of several short-term forecasting algorithms presented in Chapter 3 are highly dependent on the size of training dataset, as well as selection of their own internal parameters (called hyper-parameters). Studies in [29] and [51] used big datasets to achieve a significant performance merit. In author's view, a highly accurate short-term PV power prediction model trained with limited number of observations, and validated by integrating in an EMS for a hybrid microgrid control is lacking in literature. Therefore, the problem statement of this thesis is:

Development of an ultra-short-term forecast mechanism that predicts a Photovoltaic generator's power output. Manifest the importance of PV output power forecast by comparing the performance of physical forecasting model and multiple

mainstream machine-learning based models using key performance metrics. Integrate the PVG forecast model in a weighted energy scheduling scheme for efficient power dispatch in a hybrid microgrid.

## 2.3 Research Methodology

In this work, deterministic and statistical models of a 100kW PV-array are developed in MATLAB®. The deterministic model is based on physical parameters of a SunPower PV array as outlined in Appendix-A. The machine learning models are trained using Statistics and Machine Learning Toolbox from Mathworks. The training samples are obtained from a Tier-1 weather station installed at National University of Science and Technology (NUST), Islamabad. The weather station is a joint venture of Government of Pakistan (GoP), National Renewable Energy Laboratory (NREL) and United States Agency for International Development (USAID) [53]. The most accurate model as qualified by the performance metric is integrated in an energy management scheme for microgrid dispatch under varying climate and load conditions. The EMS is developed and implemented in Simulink using Simscape Electrical Toolbox.

## 2.4 Summary

This chapter presented the literature review of two active and overlapping research domains i.e., PV output power forecast, and energy management system. Critical analysis of the available literature is outlined; problem statement is presented and the research methodology to approach the problem is presented.

# Chapter 3

# Forecast Modeling of PV Output Power Production

## 3.1 Introduction

PVGs converts the incoming sunlight into electrical power output. However, the magnitude of instantaneous power output from a PVG is difficult to predict due to uncertain climate conditions. On a clear day a PVG is expected to produce maximum power output at noon, while moving cloud cover can significantly reduce the amount of power generated. This unpredictability creates a lot of problems for a utility grid operator, such as reverse power flow [45, 46]. Such scenarios can create undue burden on backup energy reserves of a microgrid system. Grid issues like power quality, generation control and protection are further complicated by the intermittent PVG power output. PVG integration in a microgrid is significantly inhibited if these problems are not addressed.

Safe and economic grid integration of PVG requires an accurate forecasting model for PV power output. An accurate power forecast enables grid operators to gain deeper insight of grid operation, issue commands, and optimally dispatch grid power. This chapter presents design and development of an accurate forecast

model for PVG output power. First a benchmark model is developed using elementary loadline analysis of a 100kW PVG in Simulink. Maximum power output estimation problem is formulated and a deterministic model is developed using elementary physics that governs PV power output. Machine learning workflow is used to train and validate statistical models like Matern 5/2 Gaussian Process Regression (M5/2GPR), Rational Quadratic Gaussian Process Regression (RQGPR), and Support Vector Machine (SVM). Based on Root Mean Squared Error (RMSE) as Key Performance Indicator (KPI), a model with maximum accuracy is stated.

## 3.2 Loadline Analysis

Assume that a PV-cell is operating at a constant irradiance and temperature. A loadline (as defined by a particular load) represents the point of operation (POP). Intersection coordinates of any chosen loadline with the V-I curve represents a POP. Applying an appropriate load to the PV is a critical operational element to achieve maximum PV efficiency. As indicated in Fig (3.1), if a PV-cell experiences too little load (point A) or too high load (point B) the power yield would be less than available maximum power. Output power of PV-cell is zero on x and y-intercepts of V-I curve, which represent $I_{SC}$ and $V_{OC}$ of a PV-cell respectively.

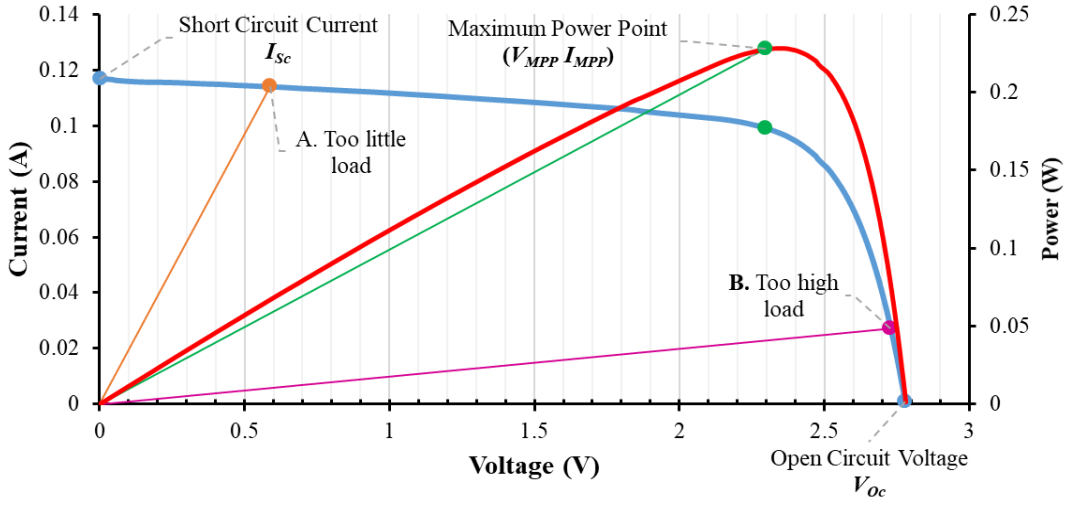


FIGURE 3.1: Loadline Analysis of a PV cell.

Circuit represented in Fig (3.2) is simulated in Simulink to perform loadline analysis, and forms basis of entire benchmarking activity in this thesis rendition. A variable AC voltage source is connected at the output terminals of a 100kW PV system. The specifications of the said PV system are outlined in Appendix-A. The variable AC voltage source is linearly varied from zero to PV's Open Circuit voltage (VOC). Consequently, the PV-system returns current and power vectors, as represented in Fig (3.1). The maximum power value in the power vector represents MPP.

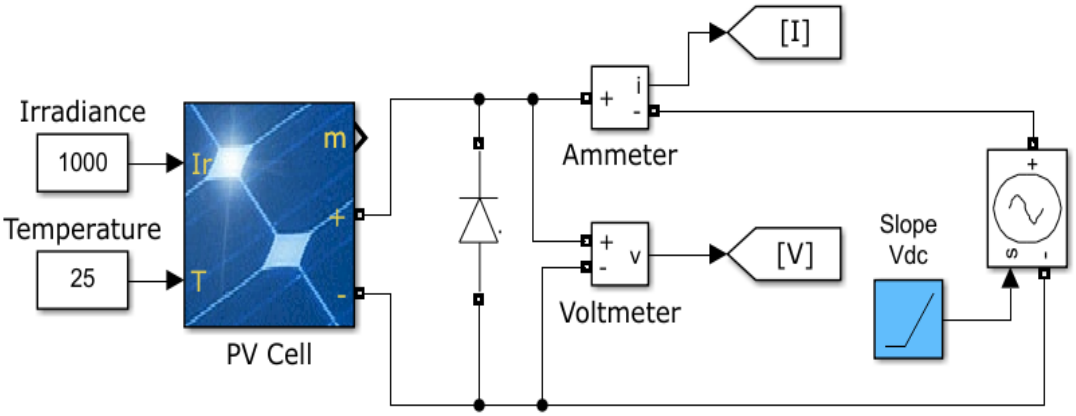


FIGURE 3.2: Circuit for Loadline Analysis.

## 3.3 PV Power Output Estimation Problem

The MPP of a PV generator chaotically changes according to varying GHI and temperature conditions, throughout the year, as depicted in Fig (3.3). For instance, MPP decreases with decreasing GHI while it increases with decreasing temperatures, and vice versa. MPP estimation against ambient climate conditions is a difficult task requiring an assistance from data science.

## 3.4 Deterministic Model of a Solar Cell

A deterministic (DTRM) model for PV power output forecast is based on the internal physical dynamics of a PV cell. The forecast quality is directly dependent

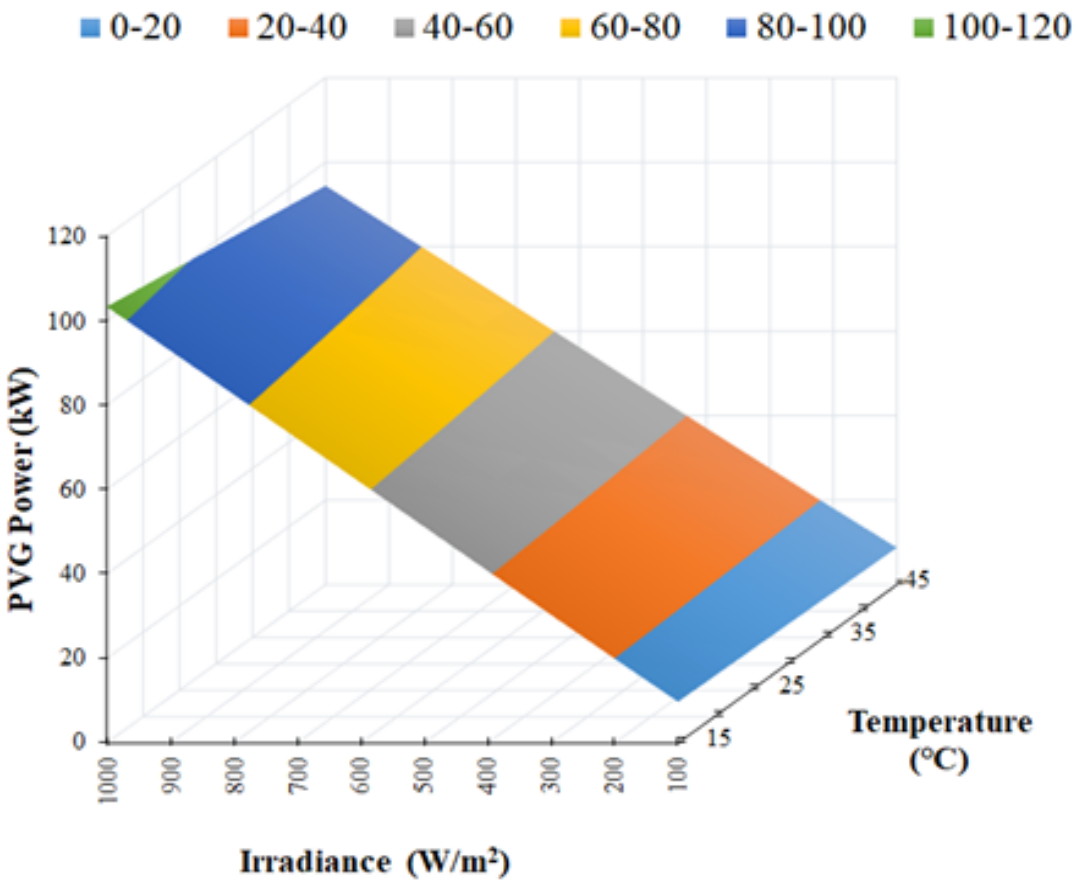


FIGURE 3.3: Surface Plot of GHI vs. Temperature vs. Maximum Power Output of a 100kW PV Generator, as Calculated from Loadline Analysis in Section 3.2.

on PV cell's fabrication limitations. Variable climate conditions further minimize forecast quality. Therefore, a careful understanding of a PV cell's band-gap energy and semiconductor temperature coefficients is necessary. The following sections summarize the impact of temperature and irradiance on a PV cell's output power. Maximum available power of a PV cell is related to the irradiance and temperature settings the PV cell is operating under. DTRM principle requires an in-depth understanding of the PV cell's equivalent circuit analysis. The location of open circuit voltage, short-circuit current and maximum available power on the volt-watt curve is very important [54].

In this study, classical five-parameter PV-cell model is used for equivalent circuit analysis. The five-parameters are solar irradiance dependent current source ($I_L$), reverse saturation current ($I_{Sat}$), diode quality factor, shunt resistances $R_{SH}$ and series resistance ($R_S$) Fig (3.4). Operation of this circuit is governed by eq (3.1)

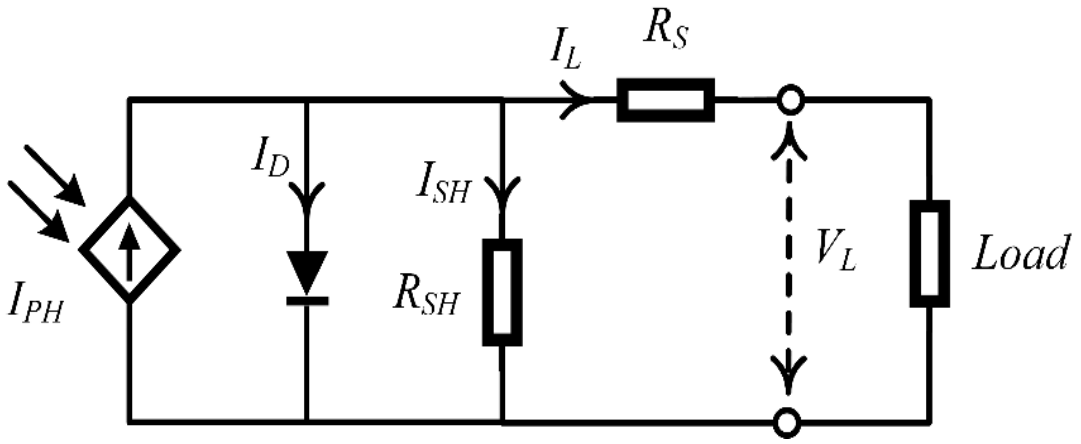


FIGURE 3.4: Equivalent Circuit Diagram of a PVG [55]

.

$$I_L = I_{ph} - (I_D + I_{SH}) \tag{3.1}$$

where $I_L$, $I_{Ph}$, $I_D$ and $I_Sh$ represent load current, PV generated photocurrent, diode current and shunt resistance current respectively.

Eq (3.2) states the current through the shunt resistance.

$$I_{Sh} = \frac{V_D}{R_{Sh}} \tag{3.2}$$

Where $V_D$ and $R_{Sh}$ are forward diode voltage and shunt resistance, as stated by eq (3.3) and respectively.

$$V_D = V_L + \frac{N_{Ser}}{N_{Par}} I_L R_{S,ref} \tag{3.3}$$

$$R_{Sh} = R_{S,ref} \left( \frac{N_{Ser}}{N_{Par}} \times \frac{S_{Ref}}{S_{Amb}} \right) \tag{3.4}$$

Parameters like $R_{Sh,ref}$ and $R_{S,ref}$ represent reference shunt resistance and reference series resistance respectively and are typically obtained from a solar panel's datasheet. $N_{Ser}$ and $N_{Par}$ represent no. of series modules and no. of parallel strings, respectively. $S_{Ref}$ is the nominal irradiance level $1000W/m^2$ while $S_{Amb}$ represents ambient irradiance value. Photocurrent $I_{Ph}$ generated by the PV cell is given by eq (3.5),

$$I_{Ph} = N_{par}(\frac{S_{ref}}{S_{Amb}})(I_{Ph,ref} + \alpha_{isc}(T_{Cell} - T_{Ref})) \tag{3.5}$$

Here $T_{Ref}$ and $T_{Cell}$ represent reference temperature $25^oC$ and cell temperature, respectively. $\alpha_{isc}$ represents temperature coefficient of photodiode's short circuit current $I_{Sc}$. $I_{Sc}$ and photodiode's open circuit voltage $V_{Oc}$ are given by eq (3.6) and (3.7) respectively.

$$I_{Sc} = I_{Sc,ref} + \alpha_{isc}(T_{Cell} - T_{Ref})) \tag{3.6}$$

$$V_{Oc} = V_{Oc,ref} + \beta_{Oc}(T_{Cell} - T_{Ref})) \tag{3.7}$$

Where $I_{Sc,ref}$, $V_{Oc,ref}$, and $\beta_{Oc}$ represent $I_{Sc}$/module, $V_{Oc}$/module, and temperature coefficient of $V_{Oc}$ respectively.

The dependence of diode's band-gap energy $\epsilon_G$ with $T_{Cell}$ is given by eq (3.8)

$$\epsilon_G = \epsilon_{G,ref}[1 + (\frac{d\epsilon_G}{dT})(T_{Cell} - T_{Ref})] \tag{3.8}$$

Here $\epsilon_G/dT$ is the slope of $\epsilon_G$ versus $T_{Cell}$ plot, and $\epsilon_{G,ref}$ is reference-band-gap-energy. Reverse saturation current $I_{Sat}$ is depicted in eq (3.9)

$$I_{Sat} = I_{Sat,ref} N_{Par}(\frac{T_{Cell}}{T_{Ref}})^3 \exp[\frac{q}{k}(\frac{\epsilon_{ref}}{T_{Ref}} - \frac{\epsilon_G}{T_{Cell}})] \tag{3.9}$$

where $I_{Sat,n}$ and q are reverse saturation current per module and charge on an electron respectively.

The forward diode current $I_D$ is given by eq

$$I_D = I_{Sat} \exp[\frac{V_D}{V_{T,ref} N_{Ser} \frac{T_{Cell}}{T_{Ref}}} - 1] \tag{3.10}$$

Substituting eq (3.2), (3.3) and (3.10) in eq (3.1) yields load current as,

$$I_L = \frac{N_{PAR} S_{Ref}}{S_{Amb}} (I_{PH,ref} + \alpha_{Isc}(T_{Cell} - T_{Ref})) - I_{Sat} \exp[\frac{V_D}{V_{T,Ref} N_{Ser} T_{Cell}/T_{Ref}}] - \frac{R_D}{R_{Sh}} \tag{3.11}$$

Deterministic product of $I_L$ with $V_L$ represents the PV output power as stated in eq (3.12) and can easily be calculated based on parameters outlined in a typical PV datasheet.

$$P_{Det} = I_L \times V_L \tag{3.12}$$

## 3.5 Regression

Regression techniques primarily deal with continuous data e.g., variation in temperature or irradiance or energy demand in an electrical grid. Typical applications range from load forecasting in an electric grid to algorithm trading.

There are a number of model types used in regression problems such as ensembles, trees etc. However, not every model type can provide enough accuracy to solve a particular problem. This thesis undertakes mainstream regression models like Linear Support Vector Machine (LSVM), Gaussian Process Regression with Rational Quadratic kernel (RQGPR) and Gaussian Process Regression with Matern 5/2 (M5/2GPR).

## 3.6 Machine Learning Roadmap

A systematic roadmap as shown in figure 3.5 is mandatory for effectively tackling a machine-learning problem [11]. In this thesis rendition, the machine-learning task is performed according to the said roadmap.

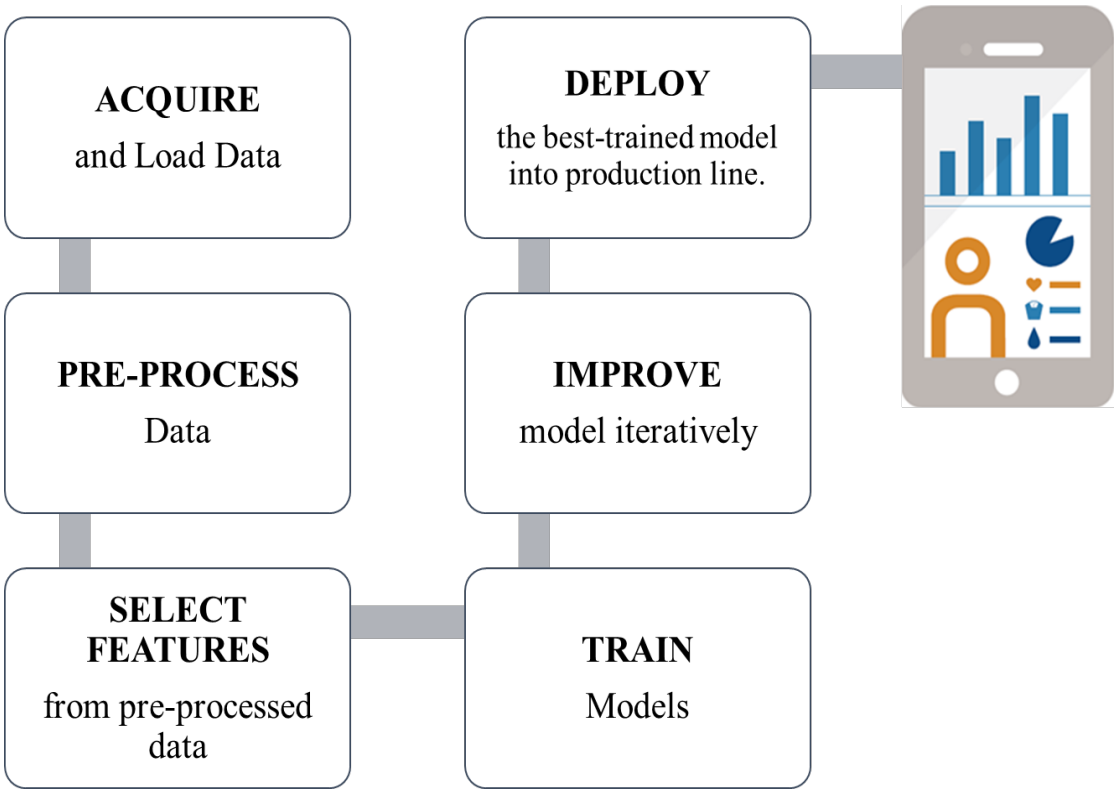


FIGURE 3.5: Machine Learning Roadmap [11].

### 3.6.1 Data Acquisition

This dissertation discusses the machine learning application to improve power prediction accuracy of hybrid microgrid systems, consisted exclusively on PV generators. Machine learning algorithms are integrated with PVG controller in order to address the problem in section 3.2. In the next chapter, a microgrid scenario with independent climate dataset recorded in Islamabad, Pakistan is discussed for the said purpose. The training dataset is labeled as Global Horizontal Irradiance (GHI), temperature and (the respective) maximum PV output power calculated from loadline simulation of 100kW PVG network as discussed in section 3.2.

#### 3.6.1.1 Dataset Description

This study undertakes climate dataset consisted of GHI and dry bulb temperature information. The data is obtained from a weather station installed at public sector university at Islamabad, Pakistan. The weather station is a collaboration since

2008, between Government of Pakistan, NREL and USAID. The weather station contains following measurement systems:

- Solys2 Tracker and CMP21 Pyranometer (by Kipp and Zonen),
- Campbell scientific CR1000 data logger,
- Temperature sensors.

Climate data is recorded at a 10-minute resolution by CR1000, and uploaded to an online data storage. The climate dataset is available at [53] for non-commercial purposes. This study uses the climate data from [53] which contains 132,259 readings of GHI and temperature. The raw climate data is recorded between October, 2014 and June, 2017, as is shown in figure 3.6. This data is clearly over-sufficient for machine learning purposes and must be pre-processed before any meaningful information is available.

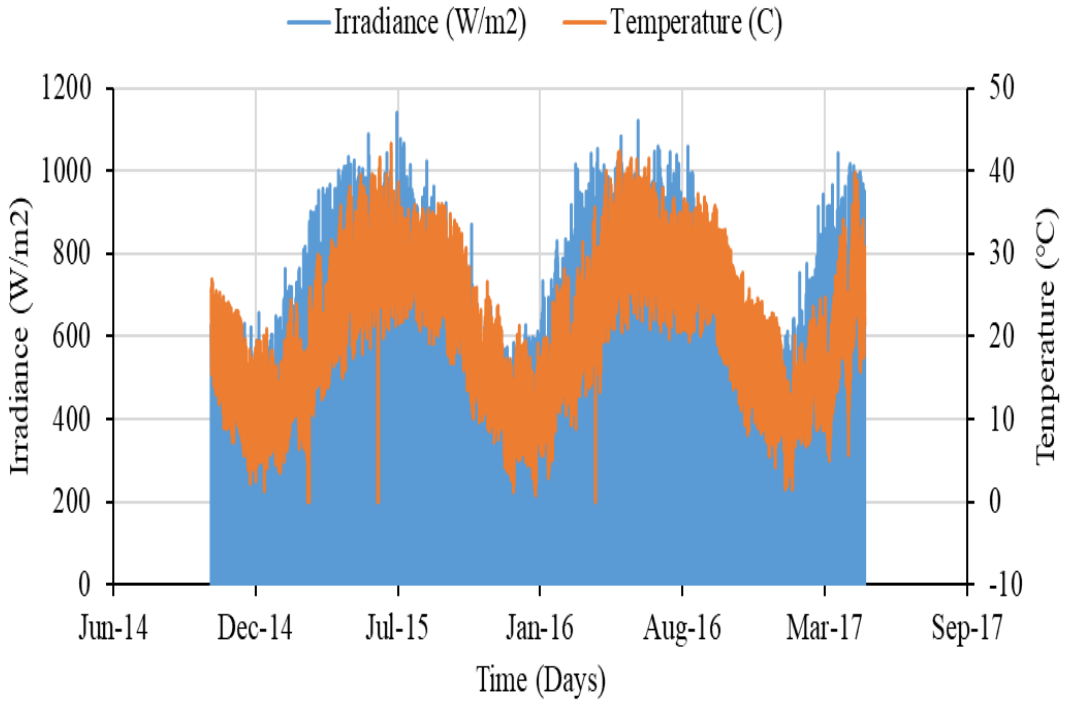


FIGURE 3.6: Islamabad Climate Dataset with Irradiance and Temperature Features as Reported Between October, 2014 and June, 2017.

### 3.6.2 Data Pre-Processing

Climate dataset shown in figure 3.6 is presented to pre-processing stage. Outliers like deviation from physical limits are isolated and night records are removed. Weights of individual climate dataset features like GHI and temperature are determined using Neighborhood Component Analysis (NCA) feature engineering technique. Five-fold cross validation is used as regularization parameter in feature selection procedure. The individual feature weights of GHI and temperature are 9.241 and 14.38 respectively. Since the feature weights are nonzero, both GHI and temperature are considered crucial for ML model design. Numerical summary of the pre-processed dataset is outlined in table 3.1.

TABLE 3.1: Numerical Summary of Dataset Obtained After Quality Control procedure.

| **No.** | **Feature /Target** | **Mean** | **Median** | **Mode** | **Min.** | **Max.** | **Range** | **Std. Dev.** |
|---|---|---|---|---|---|---|---|---|
| **1** | Irradiance ($W/m^2$) | 751.8 | 752.4 | 929.2 | 407.5 | 1140 | 732.5 | 171.5 |
| **2** | Temperature (°C) | 27.3 | 27.2 | 34.8 | 9.6 | 43.3 | 33.7 | 7.9 |
| **3** | Maximum Power ($W$) | 74,465.5 | 74,483.2 | NAN | 101 | 112,373.2 | 112,272.2 | 16,364.5 |

### 3.6.3 Feature Selection

Feature engineering or feature selection technique reduces the number of features in a model and eventually decreases the computational complexity of the overall model [61]. Feature selection is a very important tool in order to counter the overfitting problem. Pre-processed climate dataset contains two features i.e.,

- Global Horizontal Irradiance (GHI) and,

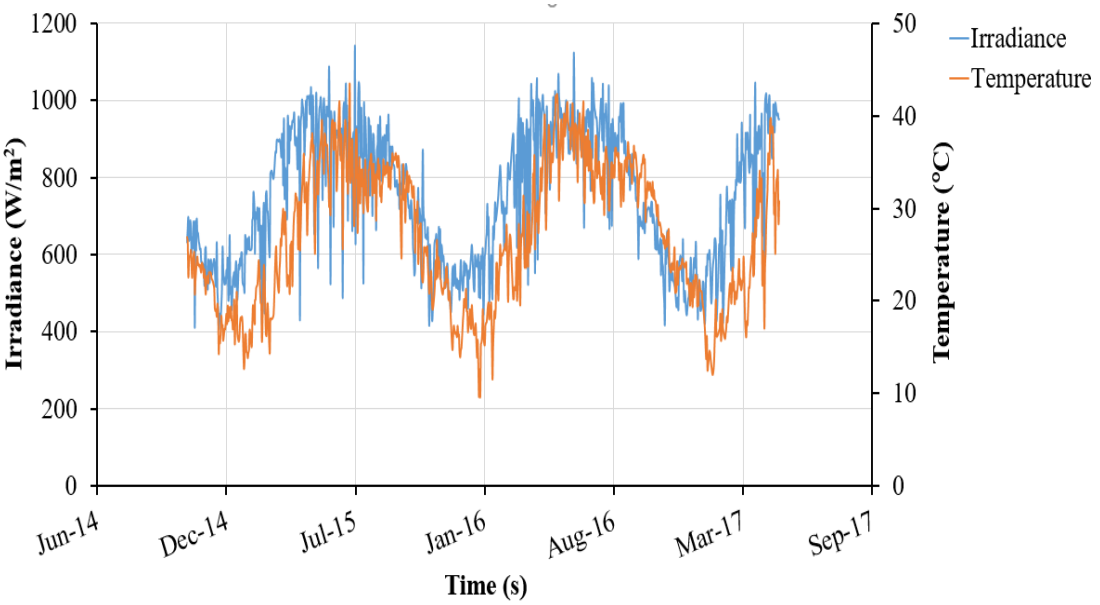


FIGURE 3.7: Pre-processed Climate Dataset.

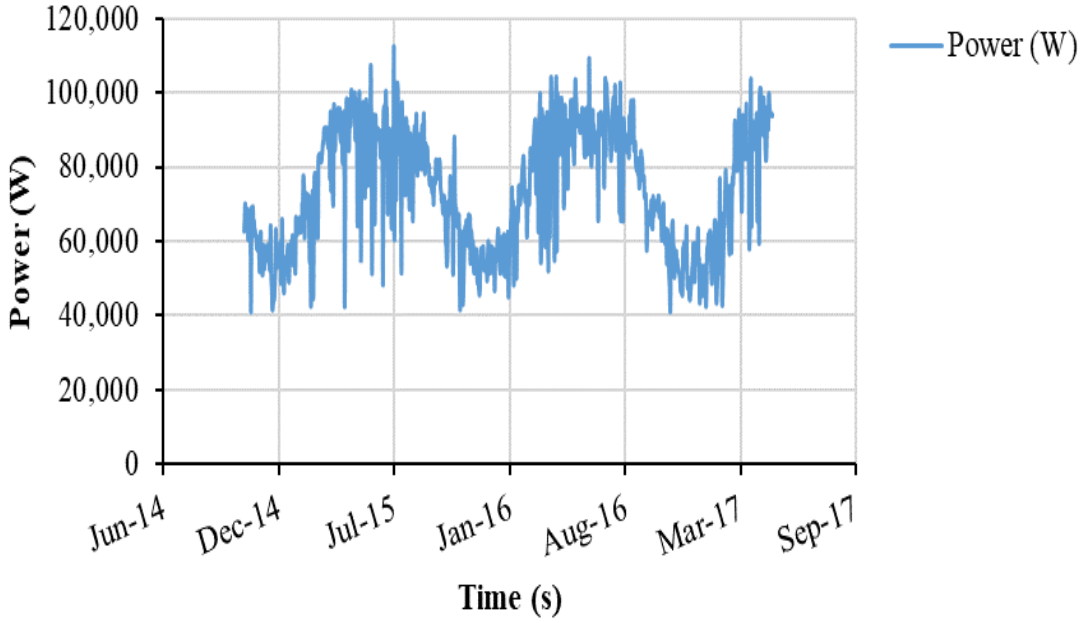


FIGURE 3.8: Maximum PVG Output Power Values as Obtained from Loadline Analysis on Pre-processed Climate Dataset.

- Air Temperature.

Since both the two features are crucial for PVG power output forecast accuracy, therefore, offsetting any one of these features deteriorates model prediction quality. Therefore, the feature-selection step is not applicable in this scenario.

### 3.6.4 Model Training

Regression models discussed in section 3.5 are individually trained using climate dataset. The dataset is mathematically represented in equation 3.13,

$$\vec{D} = [(x_j, y_j)|j = 1, ..., n] \tag{3.13}$$

where $x_j \in \mathrm{R}^2$ (GHI, temperature), $y_j \in \mathrm{R}^1$ (MPP), and $n$ = Number of Observations (856 for climate dataset). The dataset $\vec{D}$ is used to develop a generalized model, which distributes the output at unobserved input samples.

$$y = x^T\beta + \epsilon \tag{3.14}$$

where $\epsilon \sim (0, \sigma^2)$ and $\sigma^2)$ is error variance and $\beta$ is a vector of coefficients that are calculated from input training set.

### 3.6.5 Model Improvement

As discussed in section 3.5 models are iteratively trained using Statistics and Machine Learning Toolbox of MATLAB using the dataset $\vec{D}$. A model with the best error performance is used for PV power output estimation to assist the microgrid discussed in the next chapter. Statistical techniques such as Gaussian Process Regression (GPR) with Matern-5/2 and Rational Quadratic kernels, Linear Support Vector Machine as discussed in section 3.5 apply the climate dataset for PV power reserve estimation. The iteration procedure is divided into three sub-tasks i.e.,

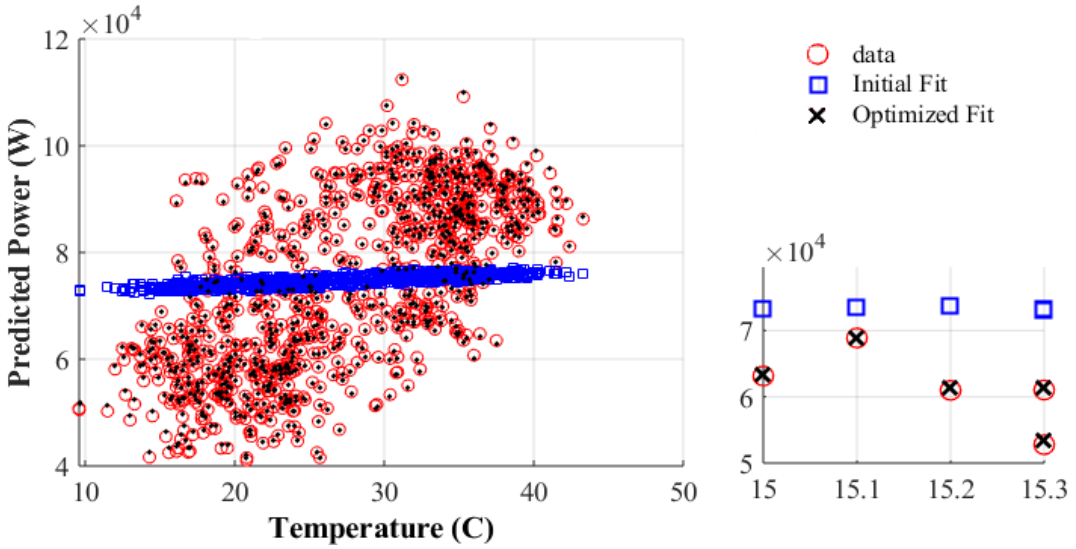


FIGURE 3.9: Optimization of LSVM Model with Temperature Predictor.

- Model Training,
- Model Validation,
- Model Testing.

The first two sub-tasks are performed simultaneously using 5-fold cross validation on the Islamabad climate data $\vec{D}$ recorded between year 2014 and 2016. The 4-folds are used for model training, while 1-fold is reserved for model validation. Testing sub-task is performed using the subset of $\vec{D}$ recorded between years 2016 and 2017. Three types of models are trained based on their respective supervised ML algorithms i.e., LSVM, M5/2GPR and RQGPR. Figure 3.9, 3.10, 3.11, 3.12, 3.13, and 3.14 present post-optimization response of LSVM, M5/2GPR and RQGPR models versus individual predictors. Impact of optimization on algorithm improvement is presented in individual inset figures. In case of LSVM in 3.9 and 3.10, the initial-fit and optimized-fit results are dissimilar; optimized results closely resemble the original data. On the other hand, the original data, initial-fit and optimized-fit results are convergent. Therefore, optimized-fit LSVM, initial-fit M5/2GPR and initial-fit RQGPR models are opted for the following steps in ML workflow.

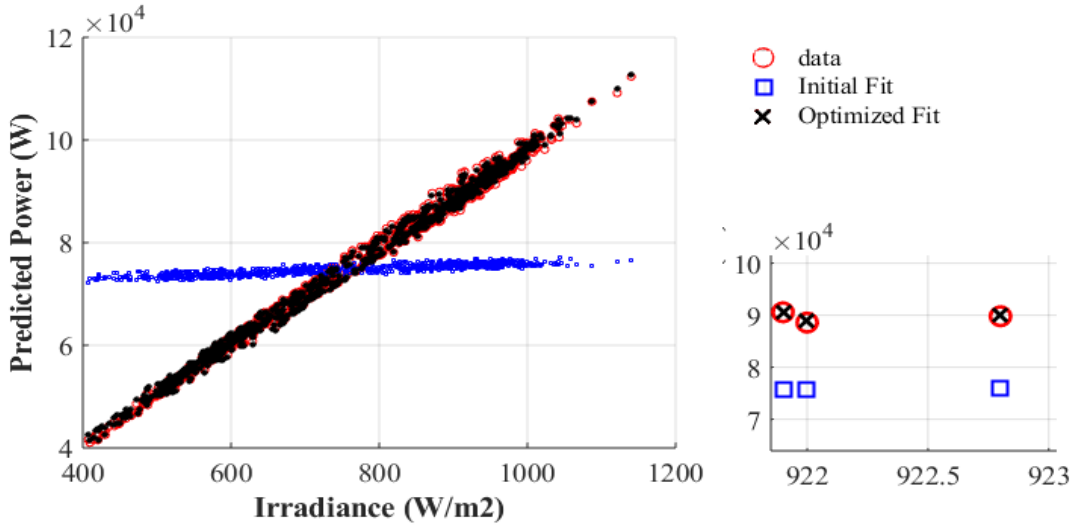


FIGURE 3.10: Optimization of LSVM Model with GHI Predictor.

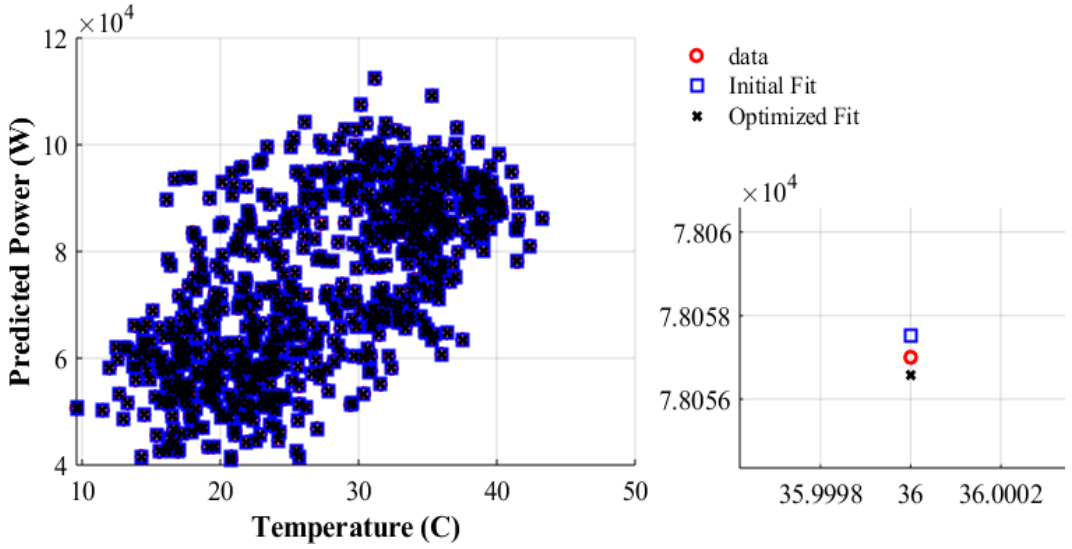


FIGURE 3.11: Optimization of M5/2GPR Model with Temperature Predictor.

Figure 3.15 presents time series plot of individual ML forecasts, along with deterministic forecast discussed in section 3.4, against benchmarking loadline data. Model forecasts in figure 3.15 are obtained using training and validation subset of $\vec{D}$, recorded between 2014 and 2016; the inset plot depicts zoomed in display of observations recorded over a period of 30 days in 2015. Model estimations in figure 3.16 are obtained using testing subset of $\vec{D}$ recorded between 2016 and 2017; the inset plot depicts zoomed-in display of observations recorded over a period of 16 days in 2017. It can be concluded from the time-series that ML estimations outperform deterministic estimation. However, it is difficult to conclude that which

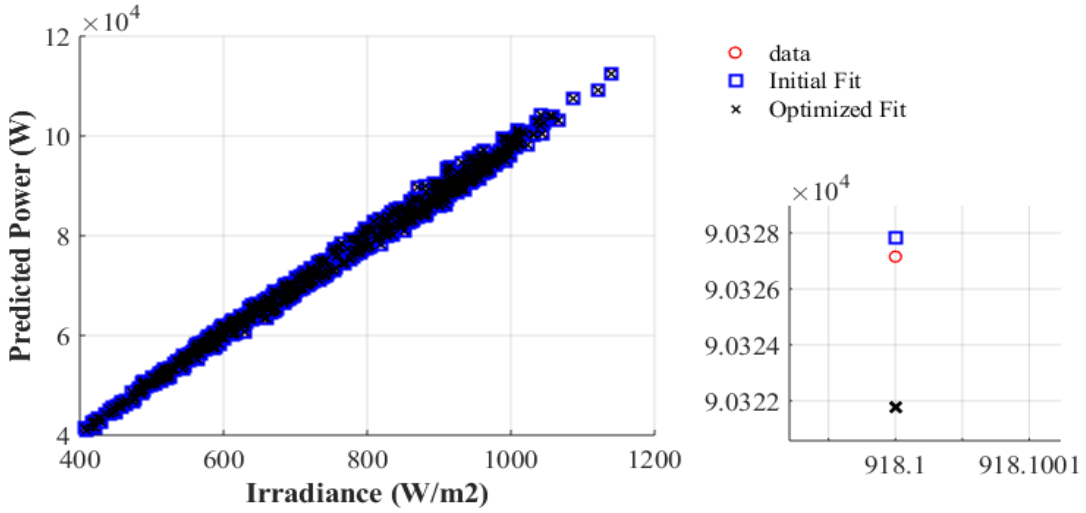


FIGURE 3.12: Optimization of M5/2GPR Model with GHI predictior.

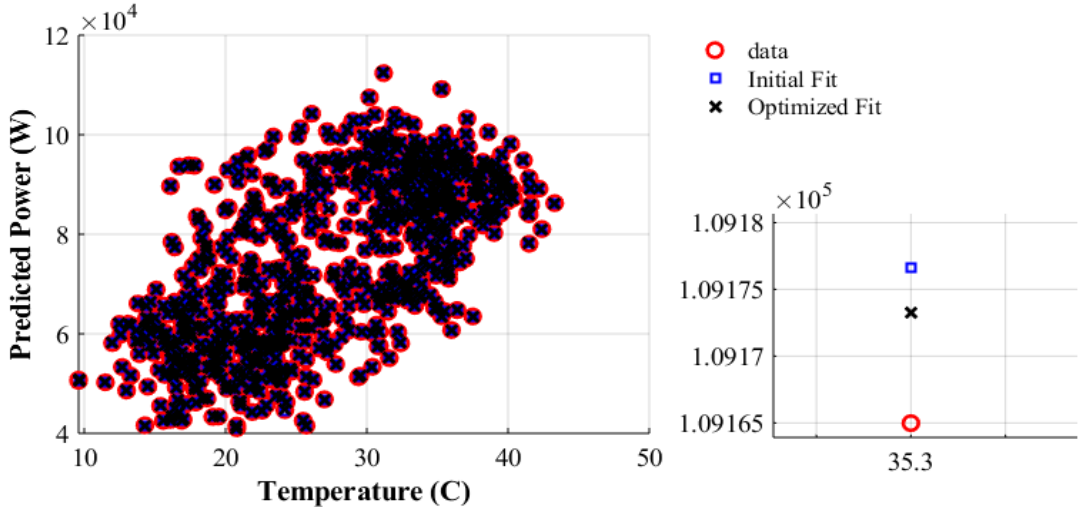


FIGURE 3.13: Optimization of RQGPR Model with Temperature Predictior.

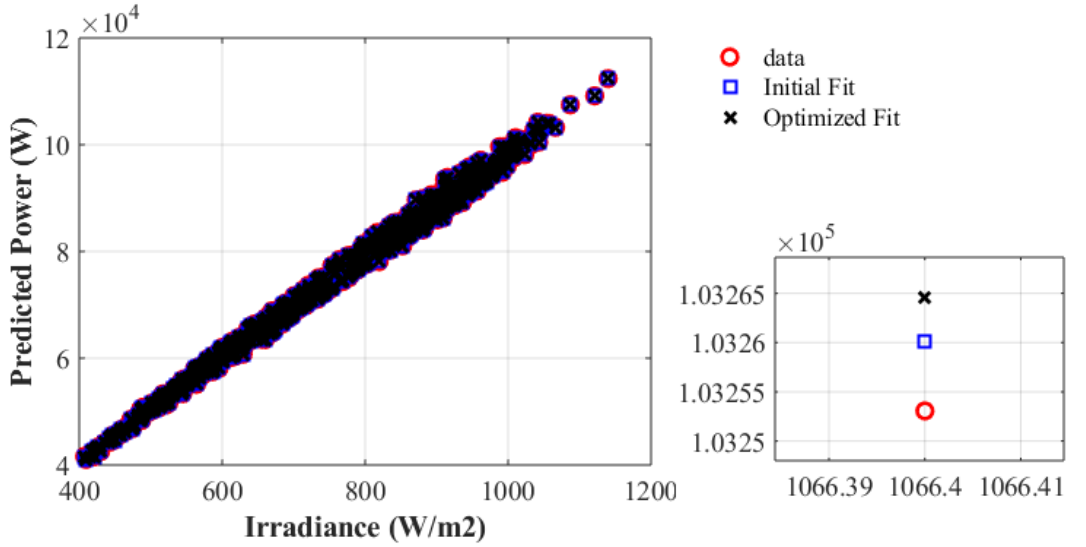


FIGURE 3.14: Optimization of RQGPR Model with GHI Predictior.

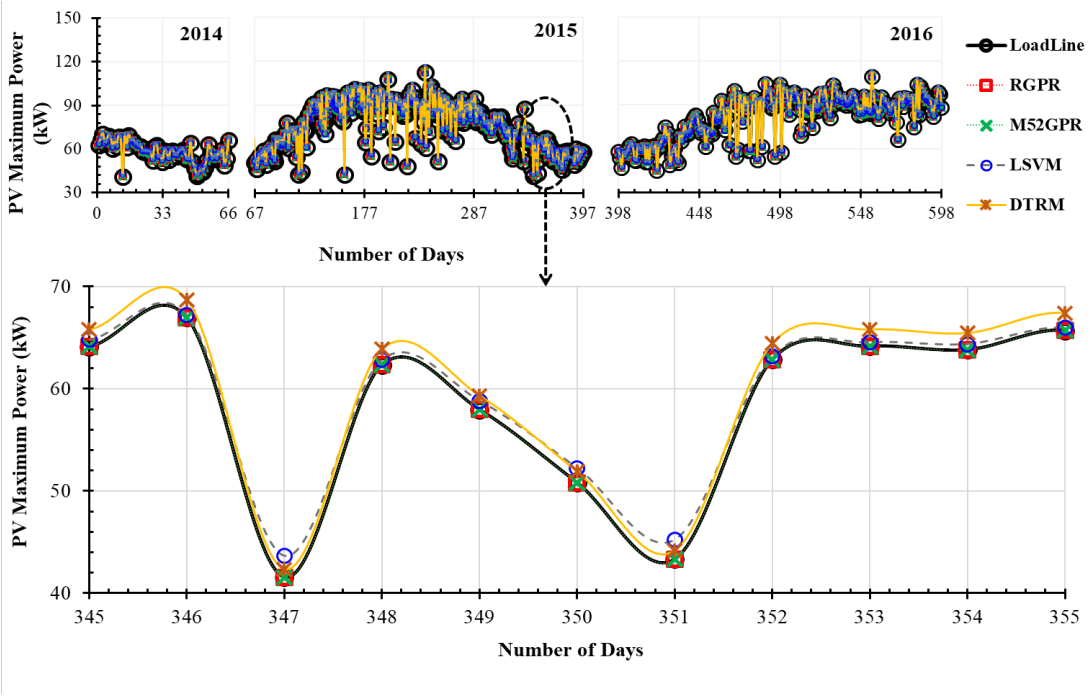


FIGURE 3.15: Training and Validation of ML Models for PVG Power Output Forecast, as Benchmarked with Loadline Analysis.

of the three ML algorithms perform better than the rest. Additional analysis is required in order to qualify an algorithm as more accurate than the other.

In this thesis, RMSE is used as a KPI to evaluate, compare and qualify each ML algorithm. Figure 3.17 and 3.18 present individual ML algorithm performance for various weather datasets recorded in Islamabad, Pakistan. Figure 3.17 presents the algorithm-seasonal-performance for training and validation subset of $\vec{D}$ while figure 3.18 presents the algorithm-seasonal-performance using testing subset of $\vec{D}$. In this study, the year-round weather distribution is as following:

- Spring – 1st March to 30th April,
- Summer – 1st May to 31st August,
- Winter – 1st November to 28th February,
- Autumn – 1st September to 31st October.

Conversely, figure 3.19 and 3.20 present algorithm performance against numerous GHI bands/limits. Figure 3.19 presents the algorithm-GHI-performance for

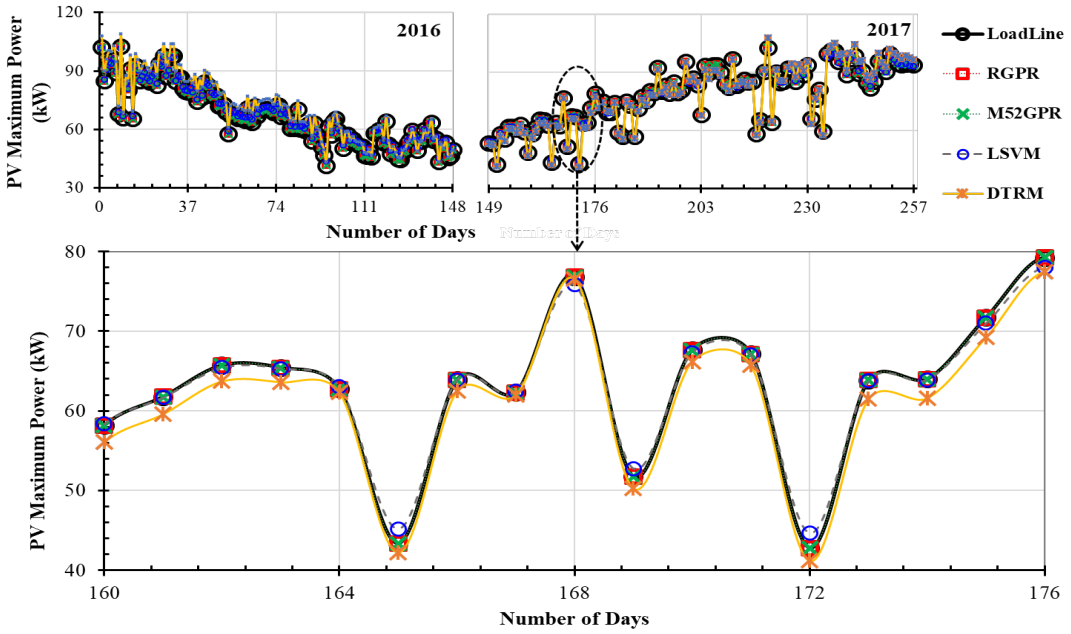


FIGURE 3.16: Testing of ML Models for PVG Power Output Prediction, as Benchmarked with Loadline Analysis.

training and validation subset of $\vec{D}$, while figure 3.20 presents the algorithm-GHI-performance for testing subset of $\vec{D}$. It can be easily concluded from visual analysis that RQGPR reported lowest RMSE for all weather and GHI distributions. Training results of all the forecasting models is illustrated in Table 3.2. It is evident that DTRM has the smallest training-time than the rest of algorithms. However, DTRM also has substantially higher forecast error and is therefore ruled out for proposed EMS presented in the next chapter. In contrast, RQGPR has a very high training-time with extremely low forecast error. Interestingly, M5/2GPR performance in terms of our KPI i.e., RMSE and training-time is between RQGPR and LSVM. A real-time PVG output power forecast application would benefit greatly from a quick-to-train M5/2GPR algorithm.

In this study the EMS design requirement declares an offline ML algorithm as adequate, therefore, M5/2GPR is no selected either. Based on the performance reflected in figures 3.15, 3.16, 3.17, 3.18, 3.19 and 3.20 and Table 3.2, RQGPR is selected for the EMS design.

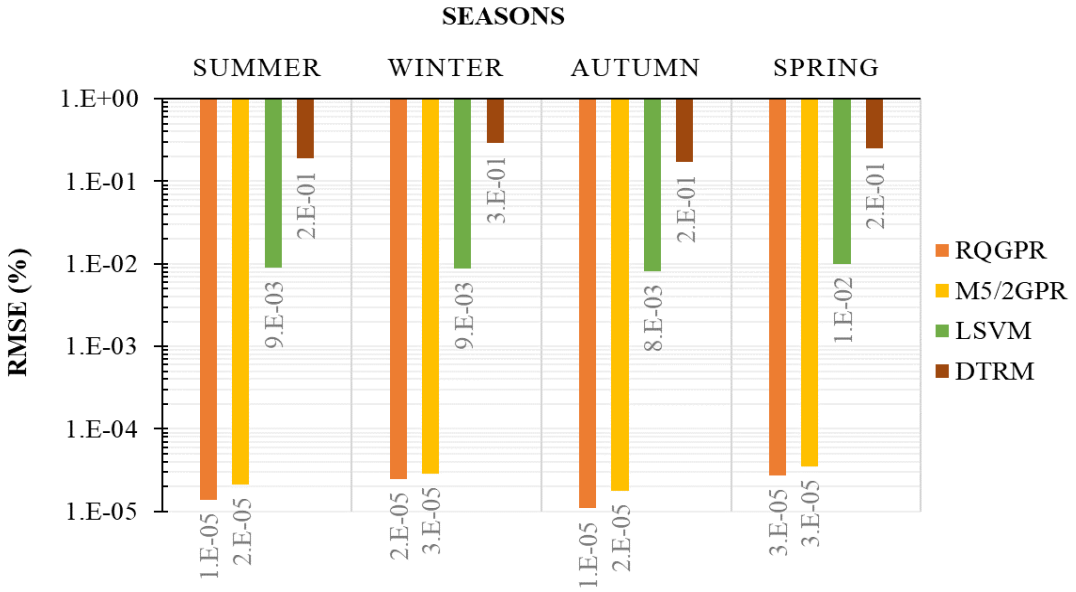


FIGURE 3.17: Seasonal Sorted, RMSE Performance Comparison of ML Techniques Computed for Training and Validation Subset of $\vec{D}$. Base Value for Percentage Error Calculation is the Rated PVG Power i.e., 100kW.

TABLE 3.2: Performance Parameters for Training and Validation Procedure.

| Technique | Time to Train (s) | MBE (W) | MAPE (%) | RMSE (W) |
|---|---|---|---|---|
| DTRM | **0** | -2363.130943 | 3.003178 | 2538.900345 |
| LSVM | 1.4511 | -410.712384 | 1.092306 | 893.957481 |
| M5/2GPR | 10.11 | 0.000062 | 0.002553 | 2.673656 |
| RQGPR | 16.9 | **0.000061** | **0.001988** | **2.085560** |

Incorporation of unmodeled PV dynamics in future can lead to more accurate ML models, for round the year microgrid service [62].

### 3.6.6 Model Deployment

The model selected in section 3.6.5 is deployed in a hybrid microgrid application, as discussed in Chapter 4. Selected model is responsible for carefully predicting the amount of power available in a PVG against particular climate conditions and assist in grid restoration.

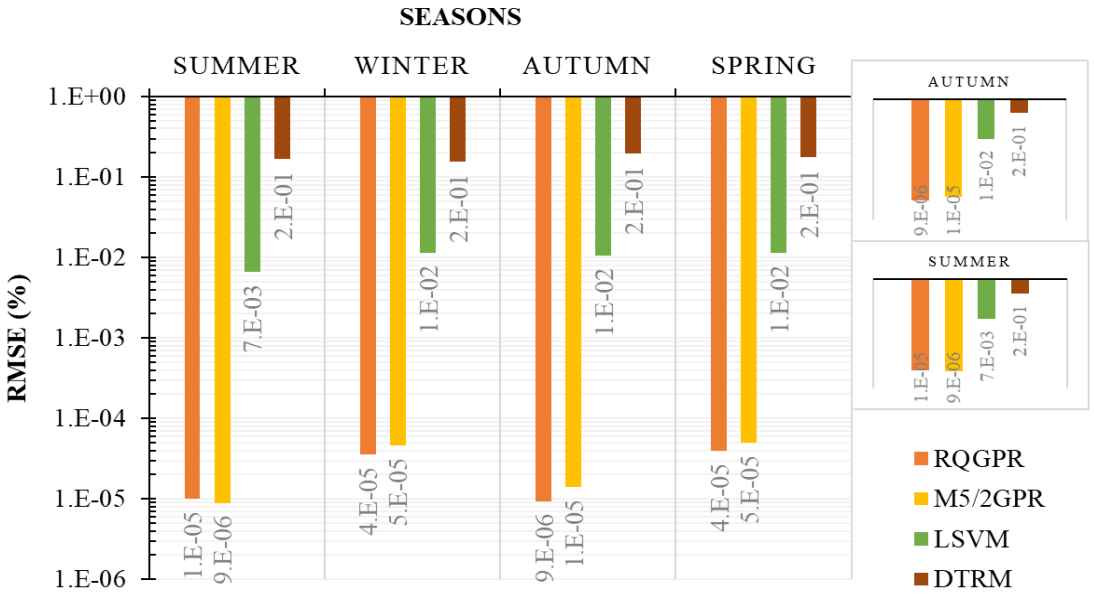


FIGURE 3.18: Seasonal Sorted, RMSE Performance Comparison of ML Techniques Computed for Testing Subset of $\vec{D}$. Base Value for Percentage Error Calculation is the Rated PVG Power i.e., 100kW.

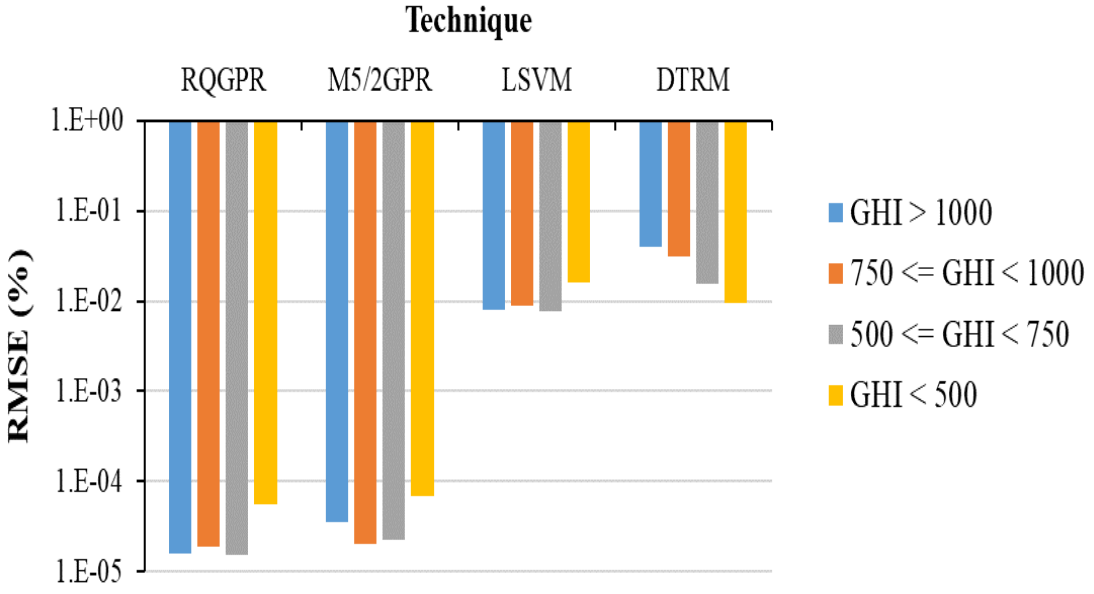


FIGURE 3.19: GHI sorted, RMSE Performance Comparison of ML Techniques Computed for Training and Validation Subset of $\vec{D}$. Base Value for Percentage Error Calculation is the Rated PVG Power i.e., 100kW.

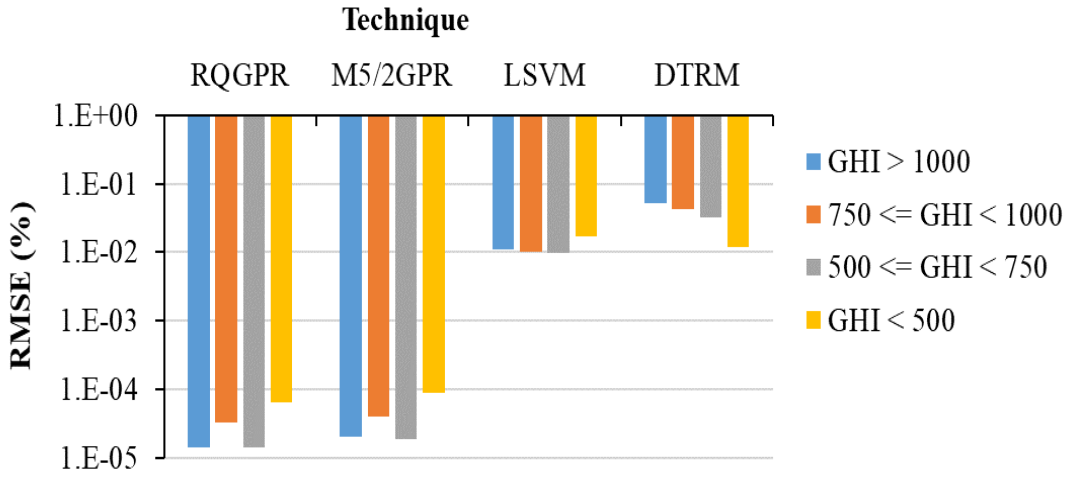


FIGURE 3.20: GHI Sorted, RMSE Performance Comparison of ML Techniques Computed for Testing Subset of $\vec{D}$. Base Value for Percentage Error Calculation is the Rated PVG Power i.e., 100kW.

## 3.7 Summary

This chapter presented forecast modeling of PV power production for a particular set of atmospheric conditions. A benchmark model using elementary loadline analysis of a 100kW PVG is developed. Deterministic model of the said PVG is also developed using classical 5-parameter modeling of a solar cell. Theoretical background of Regression algorithms used for training machine learning (ML) models is presented. A standard ML workflow is used to develop and optimize ML models like Linear Support Vector Machine (LSVM), Gaussian Process Regression (GPR) with Rational Quadratic kernel, and GPR with Matern 5/2 kernel. A climate dataset acquired at weather station installed at National University of Science and Technology (NUST) Islamabad, Pakistan., is used to train the said machines. After several iterations of model improvement, GPR with RQ kernel is declared as the most accurate equivalent of 100kW PVG.

# Chapter 4

# Application of PV Power Forecast in a Hybrid Microgrid

## 4.1 Introduction

Hybrid microgrid is a cluster of various power sources like distributed generators (DGs), energy storage systems, loads and an array of monitoring and protection devices [63]. Overall energy efficiency in a utility grid greatly improves after microgrid interaction [64]. Additionally, a hybrid microgrid significantly promotes consumption of indigenous energy resources like wind, biomass and solar, paving way to diminished environmental pressure. Microgrid interaction with the utility grid results in two operation modes, i.e., islanded mode and grid-connected mode [65]. Microgrid management is an emerging field due to vast deployment of intermittent renewable energy sources and increased diversity in loads [66]. Microgrid management is important for a number of grid requirements such as supply-demand balance, minimize operational costs and emissions, and demand-side load management [67, 68]. Another important example of grid requirement is improvement of grid stability through optimal dispatch of power generation sources in a hybrid microgrid scenario. Implementation of optimal dispatch for renewable energy based DGs hugely depends on estimation of maximum available

power, which that DG can commit. This is a challenging task due to the intermittent nature of popular renewable resources e.g., wind is not always blowing, and sun is not always shining. The intermittency problem is addressed by complementing the microgrid with energy storage systems (ESS) and electric vehicles [69]. This chapter presents a PV integrated microgrid scenario in the backdrop of multiple maximum power estimation techniques as discussed in previous chapter. This chapter resumes from section 3.6, by integrating the best-selected model in a microgrid architecture. The importance of power prediction quality in terms of microgrid stability during grid events like frequency deviation are explored.

## 4.2 System Description

This study presents design of an Energy Management Scheme (EMS) for a sample hybrid microgrid. As shown in figure 4.1 and table 4.1, the sample microgrid is consisted upon a 100kW baseload, a 10kW auxiliary load, a 100kW PV generator, a 10kAh battery storage, and a 75kW diesel generator. Sample microgrid is interfaced with a 25kV/50Hz Medium Voltage (MV) grid at the point of common coupling (PCC). The 25kV grid is categorized as an MV bus [70]. The grid architecture is designed, implemented and simulated in MATLAB/Simulink.

TABLE 4.1: List of Microgrid Components in Figure 4.1.

| No | Component Name | Type | Symbol | Value | Units |
|---|---|---|---|---|---|
| **1** | PV Generator | Source | $P_{MPP}$ | 100 | kW |
| **2** | Battery Storage | Source | $P_{STO-OUT}$ | 10 | kAh |
| **3** | Diesel Generator | Source | $P_{base}$ | 75 | kW |
| **4** | Utility Grid | - | - | $\infty$ | kW |
| **5** | Baseload | Load | $P_{Load}$ | 75 | kW |
| **6** | Auxiliary Load | Load | - | 10 | kW |

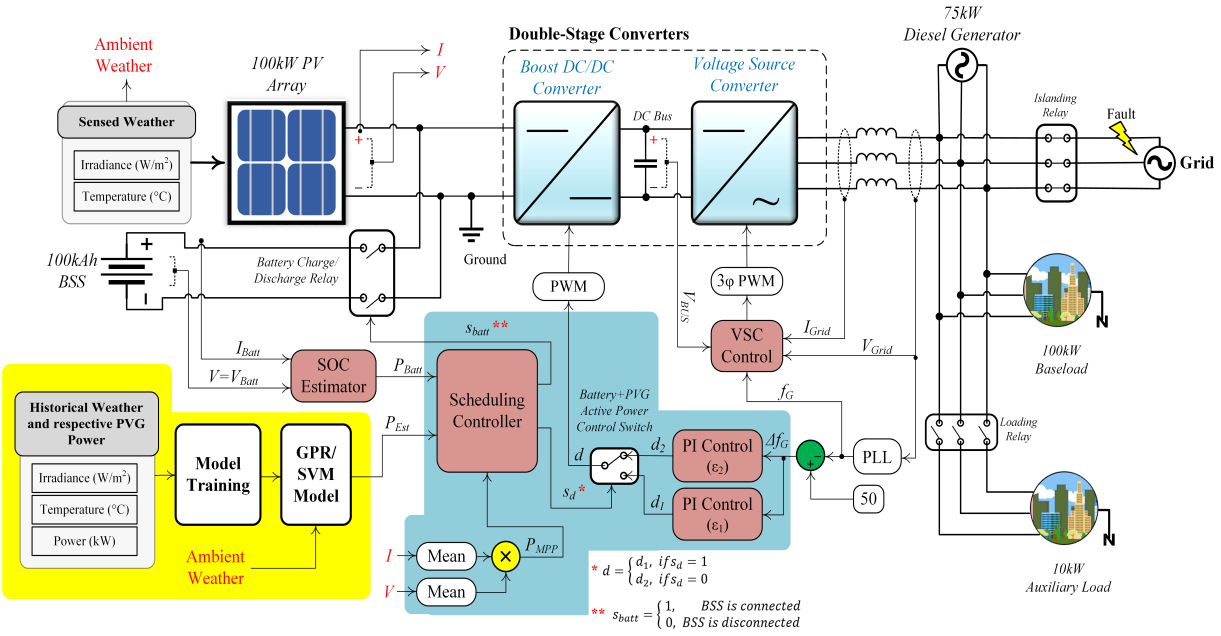


FIGURE 4.1: Block Diagram of Sample Hybrid Microgrid with Complete Schematic Components.

In *grid-connected state* the PVG produces its maximum rated output i.e., MPP, and is used to charge the Battery Storage System (BSS). Initially, BSS's State of Charge (SOC) is maintained at 80%. In grid-connected state, the diesel generator powers the baseload. In islanded state, the grid is restored by concerted efforts of diesel generator and PVG. Section 4.4 presents a detailed description of various operational states. The 100kW PV-array in figure 4.1 accepts GHI and temperature inputs and produces an unregulated current (I) and voltage (V) outputs in accordance with VI-characteristics. The 10kAh BSS is also connected to the unregulated V-bus. The PV-array is immediately followed by a double-stage converter system comprised of a boost DC/DC converter and a Voltage Source Converter (VSC). The DC/DC converter stage is responsible for MPPT, whereas VSC stage establishes utility grid interface. The proposed EMS controls the DC/DC converter using IC algorithm discussed in section 1.5.1. The IC algorithm drives the DC/DC output using a Pulse Width Modulation (PWM) signal. The VSC is controlled by a three-phase sinusoidal PWM signals. As a result, the VSC produces three-phase voltages and currents, in sync with MV-grid's frequency ($f_g$). A Phase-Locked-Loop (PLL) circuit is used to measure $f_g$. The maximum power

forecast mechanism for 100kW PVG accepts the same GHI and temperature values, as used by the PV-array to produce unregulated current (I) and voltage (V) outputs. EMS uses the forecasted power value to switch between BSS and PVG, according to the fluctuations in $f_g$.

## 4.3 Energy Management Scheme

The Energy Management Scheme (EMS) is designed to effectively counter microgrid contingency events. According to [23, 24], grid contingency events occur due to differences in grid power demand and supply. This difference is measured by magnitude of $f_g$ deviating from its nominal value (50Hz in Pakistan). Microgrid's ability to keep $f_g$ deviations within a permissible limits is called inertia [71]. Severe power imbalance can trigger blackouts in the absence of grid inertia. Equation 4.1 depicts total power output generated by microgrid sources for baseload and/or the grid (depending upon the operational state).

$$P_{Out} = k_{base}P_{base} + \epsilon_1 P_{MPP} + \epsilon_2 P_{STO-Out} \tag{4.1}$$

Here,

- $P_{base}$ is controlled by coefficient $k_{base}$,
- $P_{MPP}$ is controlled by coefficient $\epsilon_1$ with limits $[0, 1]$,
- $P_{STO-Out}$ is controlled by coefficient $\epsilon_2$ with limits $[-1, 0]$,

Coefficients $\epsilon_1$ and $\epsilon_2$ are individual gains of a dedicated Proportional Integral (PI) controller. In grid-connected state, PVG exclusively charges BSS, while the diesel generator supplies energy to the baseload and utility grid. In this state, equation 4.1 modifies into 4.2 i.e.,

$$P_{Out} = k_{base}P_{base} \tag{4.2}$$

In *grid-connected state*, $P_{STO-in}) = P_{PV} = P_{MPP}$ and $P_{STO-out} = 0$. In other words, the coefficient $\epsilon_1 = 1$ and therefore, the PVG is operating at MPP. It is important to highlight the fact that $P_{MPP}$ is the forecasted maximum PVG output power obtained from RQGPR based estimator. For more details on RQGPR refer to section 3.6.6. In *islanding-state*, EMS measures frequency error ($\Delta f_g$) from nominal value of 50Hz. The grid power imbalance is proportional to $\Delta f_g$, as represented mathematically in equation 4.3:

$$P_{Load} - P_{Out} = P_{IMB} \propto f_g \tag{4.3}$$

Immediately after islanding state, the EMS starts comparing $P_{MPP}$ with a fixed threshold (in this case 50%). As soon as $P_{MPP}$ drops below threshold limit, EMS enters *low-PV-islanded energy state*. In this state EMS summons BSS to discharge and restore grid balance. BSS is discharged when the unregulated V-bus is below the BSS nominal voltage (+200V). In this case the power equation 4.1 modifies into equation 4.4:

$$P_{Out} = k_{base}P_{base} + \mid \epsilon_2(P_{MPP} + P_{STO-out}) \mid \tag{4.4}$$

On the other hand if $P_{MPP}$ is above the threshold limit then the EMS is in *high-PV islanded energy state*. In this state BSS neither charges nor discharges; SOC of the BSS is kept at the same level as when EMS entered islanding state, i.e., $P_{STO-in} = P_{STO-out} = 0$. PVG alongside the diesel generator restores or maintains the microgrid balance. The power equation 4.1 modifies into 4.5:

$$P_{Out} = k_{base}P_{base} + \epsilon_1 P_{MPP} \tag{4.5}$$

Figure 4.2 presents the flowchart of EMS:

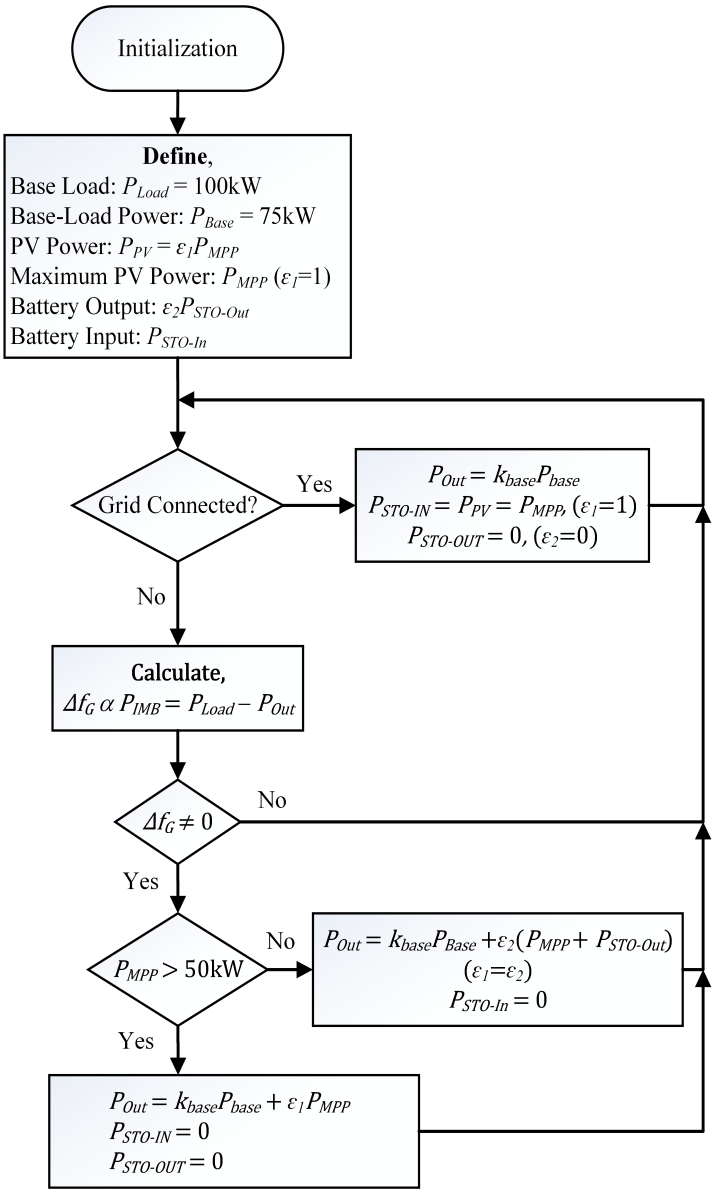


FIGURE 4.2: Flowchart of Energy Management Scheme.

## 4.4 Simulation Results

This study proposes a microgrid management strategy that effectively switches between four states i.e., grid-connected, islanding, low-PV-islanded energy, and high-PV-islanded energy states. Table 4.2 and figure 4.3 summarize switching conditions, and status or roles played by individual energy sources. This section presents the results of simulated contingency events for the sample hybrid microgrid.

TABLE 4.2: List of EMS States and Status/Roles Played by Individual Energy Sources.

| State | State Title | PVG | BSS | Diesel Generator |
|---|---|---|---|---|
| **1** | Grid-Connected | Charge BSS at MPP. | SOC is rising. | |
| **2** | Islanding | Stop BSS charging. Provide grid frequency support. | SOC is at a constant level. | Operating at an optimal value for |
| **3** | High-PV-Islanded Energy | Provide grid frequency support. | SOC is at a constant level. | microgrid support. |
| **4** | Low-PV-Islanded Energy | Provide grid frequency support. | SOC is dropping. Provide grid frequency support | |

### 4.4.1 State-1: Grid-Connected

Initially, the microgrid is connected to the utility grid and the baseload receives active power from the utility grid exclusively. The microgrid operation is controlled by the power equation 4.2. As mentioned in table 4.2, the PVG is charging BSS by operating at MPP, and diesel generator is powering the utility grid as well as baseload. In this state, active power contribution from PVG and BSS is virtually zero, as shown in figure 4.10. Figure 4.6 displays negative power output from BSS, which means batteries are charging. As a result, SOC of the BSS is rising from initial level of 80% as shown in figure 4.9.

### 4.4.2 State-2: Islanding

Islanding protocol is initiated by the EMS right after utility grid experiences a phase-to-phase short circuit fault. The fault is immediately isolated by circuit breakers. A subsequent microgrid imbalance creates a drop in grid-frequency value as depicted in figure 4.5. EMS stops BSS from charging as represented by zero energy flow in figure 4.6, and removes energy imbalance using the active power

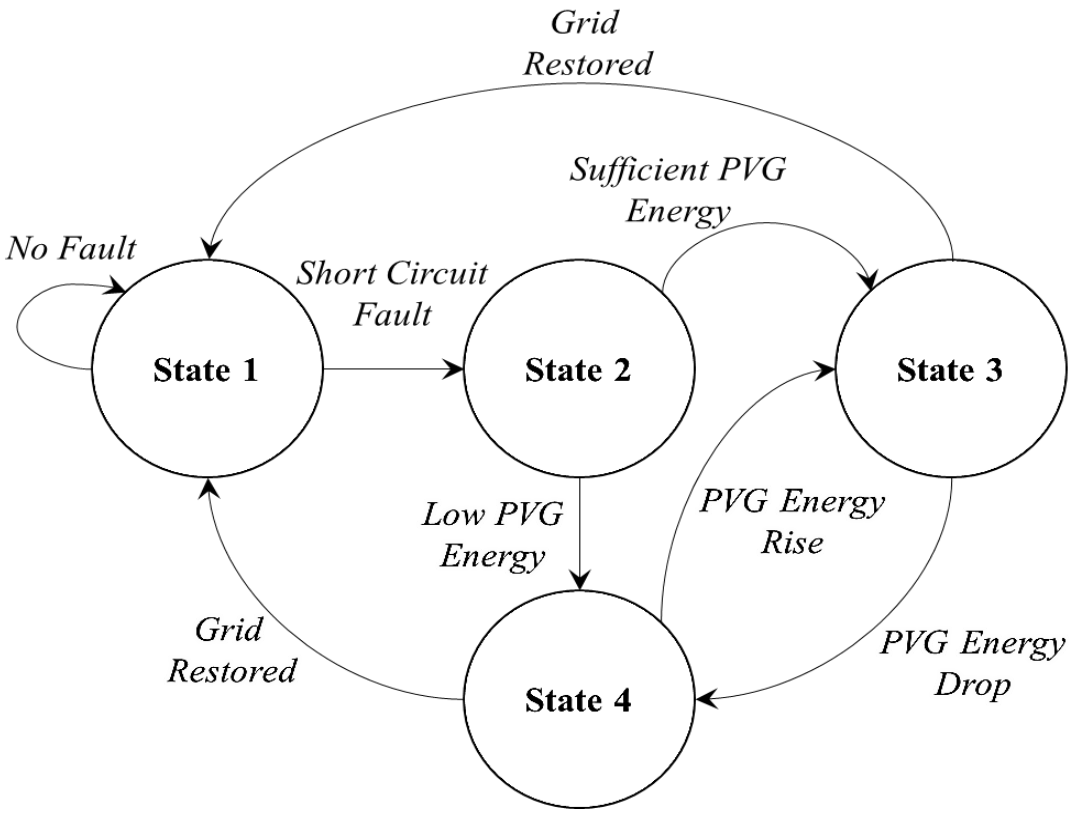


FIGURE 4.3: State Diagram for Proposed EMS.

contribution of diesel generator and PVG as shown in figure 4.10 and 4.11, respectively. Grid frequency is restored at nominal value of 50Hz as shown in figure 4.5, at the end of state-2.

### 4.4.3 State-3: High-PV-Islanded Energy

After stat-2, EMS tracks potential grid disrupting climate-conditions and energy-demand. A drop in GHI and temperature shown in figure 4.4, between time $t = [5s, 25s]$ is deliberately introduced in simulation. As a result, grid frequency deviation represented by $\Delta f_g \neq 0$ is reported in figure 4.5. More specifically, the reason for $\Delta f_g \neq 0$ is due to reduced $P_{MPP}$ and shown in figure 4.6. However, as long as $P_{MPP}$ is greater than the threshold limit discussed in section 4.4.3, BSS does not release any energy. EMS is still able to keep grid stable without BSS during an auxiliary loading event at time $t = 20s$ as shown in figure 4.5 and 4.9. It is important to state the significance of an accurate PVG output power forecast,

without which EMS can incorrectly trigger BSS and enter state-4 as discussed in sub-section 4.4.4.

A VSC produces a constant amplitude sine-wave output voltage if its input voltage is a constant DC bus. It is shown in figure 4.8 that a constant DC bus voltage of +500V withstands during states 1, 2, and 3. The DC bus remains constant regardless of DC/DC converter's input voltage fluctuations shown in figure 4.7 due to climate conditions. Figure 4.10 shows active power, whereas figure 4.11 shows reactive power from VSC into the grid. In this state, RMS grid voltage, grid frequency and THD remain voltage disturbances standard EN 50160 [72] compliant; plots are shown in figures 4.12 and 4.13. After utility grid reconnects, the Microgrid returns to state-1.

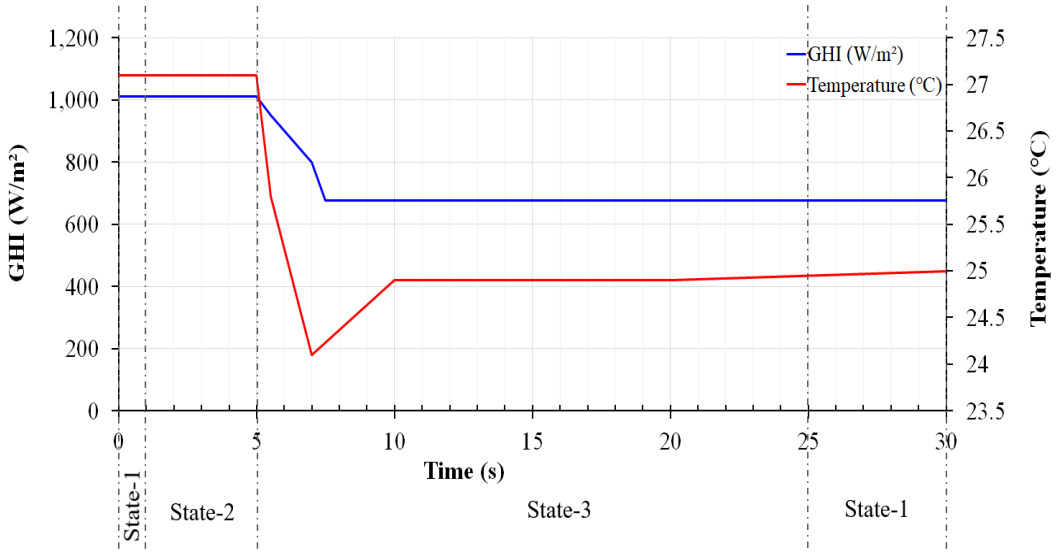


FIGURE 4.4: Simulated GHI and Temperature Profile in State-3 of Proposed EMS.

### 4.4.4 State-4: Low-PV-Islanded Energy

This state is specifically designed for severely low PVG output energy level, as observed at dusk or dawn. As concluded in section 3.4, PVG energy level decrease with decreasing GHI and increasing temperature conditions. PVG energy is deliberately driven below the threshold limit discussed in section 4.4.3 using climate

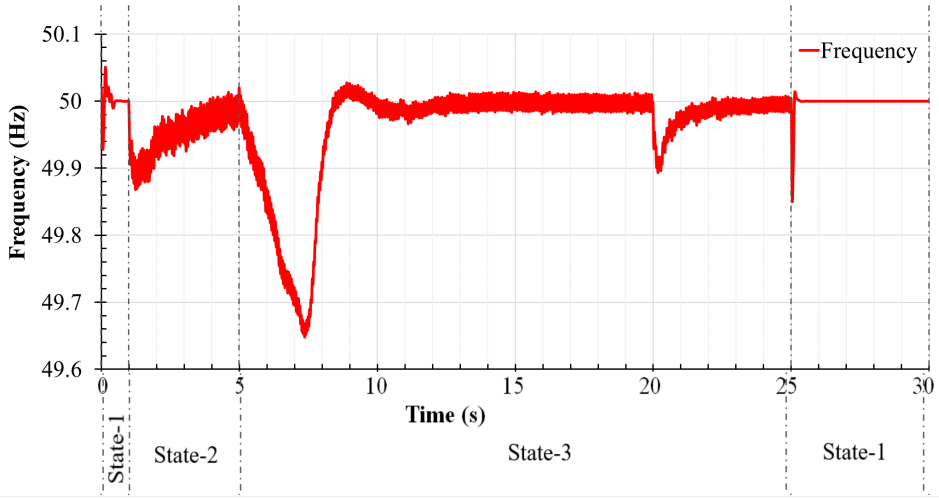


FIGURE 4.5: Grid Frequency Chart for State-3 Operation.

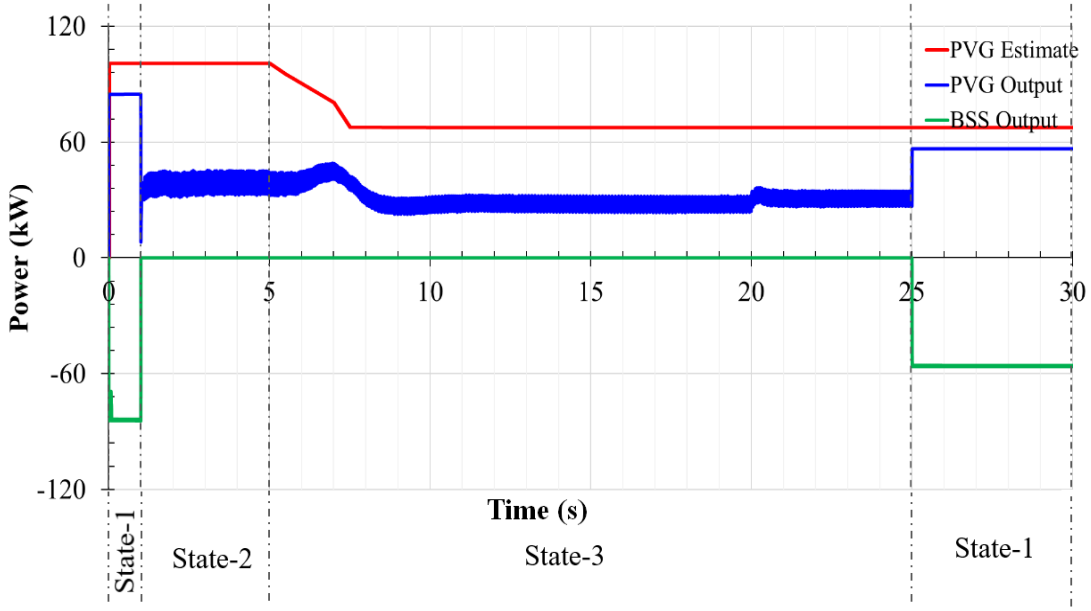


FIGURE 4.6: PVG's Forecasted and Feedback DC Power, and Battery Storage System Output Power for State-3 Operation.

profile presented in figure 4.14 . Consequently, EMS officially enters state-4. For the sake of continuity, EMS is deliberately kept in state-3. The deployed PVG output power estimator as presented in section 3.6.6, notifies EMS about drastic loss of energy supply. As a result, EMS hastily moves BSS in lower output voltage range, as illustrated in figure 4.16. Subsequently, BSS discharges and its SOC level decreases, as shown in figures 4.16 and 4.17. In the end, grid frequency stabilizes at nominal level of 50Hz as depicted in figure 4.15 and grid is restored. The grid frequency fluctuations are EN-50160 quality standard compliant [72].

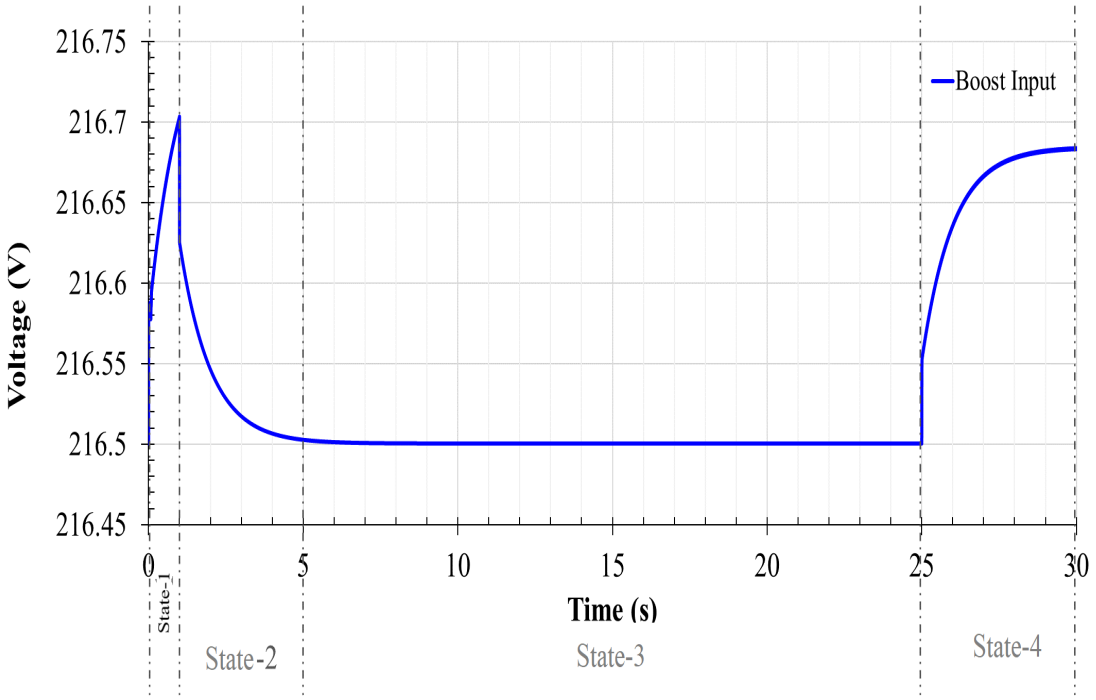


FIGURE 4.7: DC/DC converter Stage's Input Voltage for State-3 Operation.

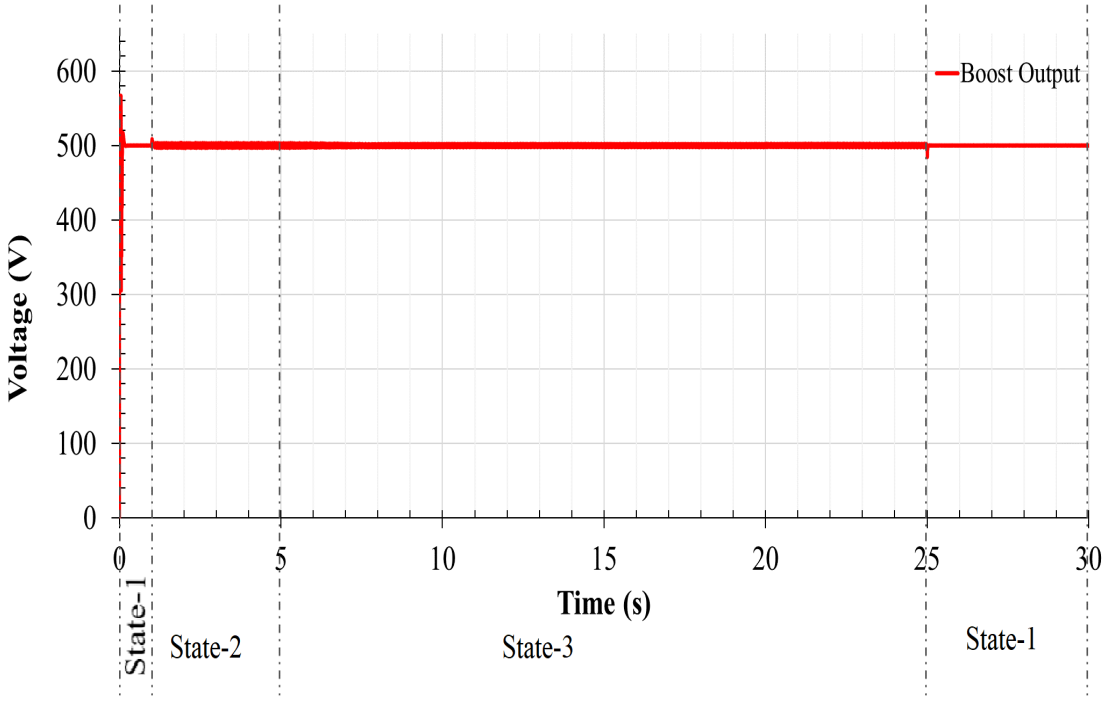


FIGURE 4.8: DC/DC Converter Stage's Output Voltage for State-3 Operation.

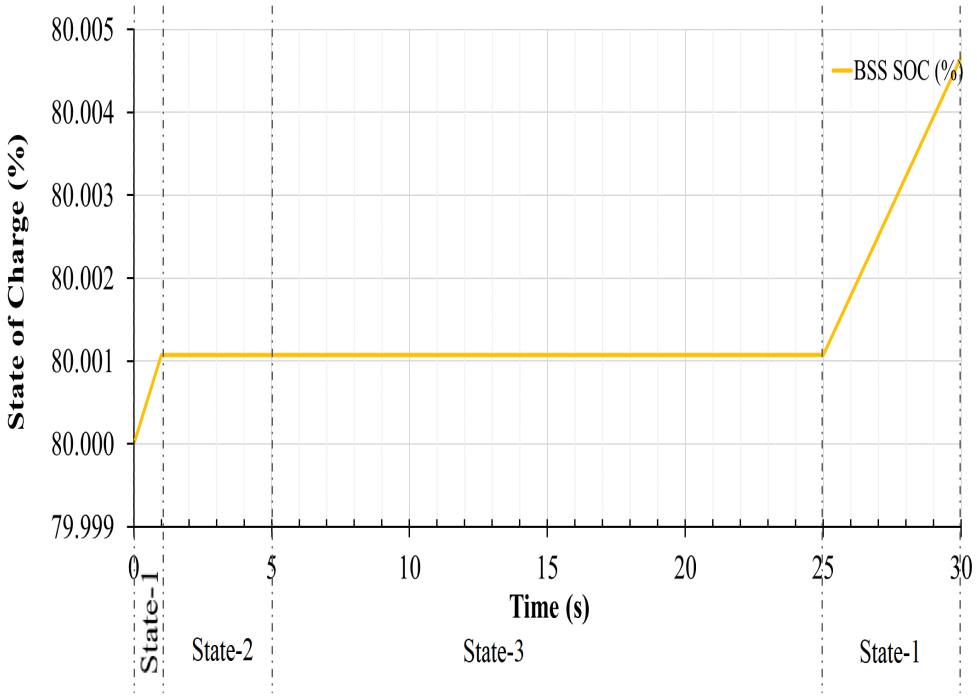


FIGURE 4.9: State of Charge (SOC) Level for BSS During State-3 Operation.

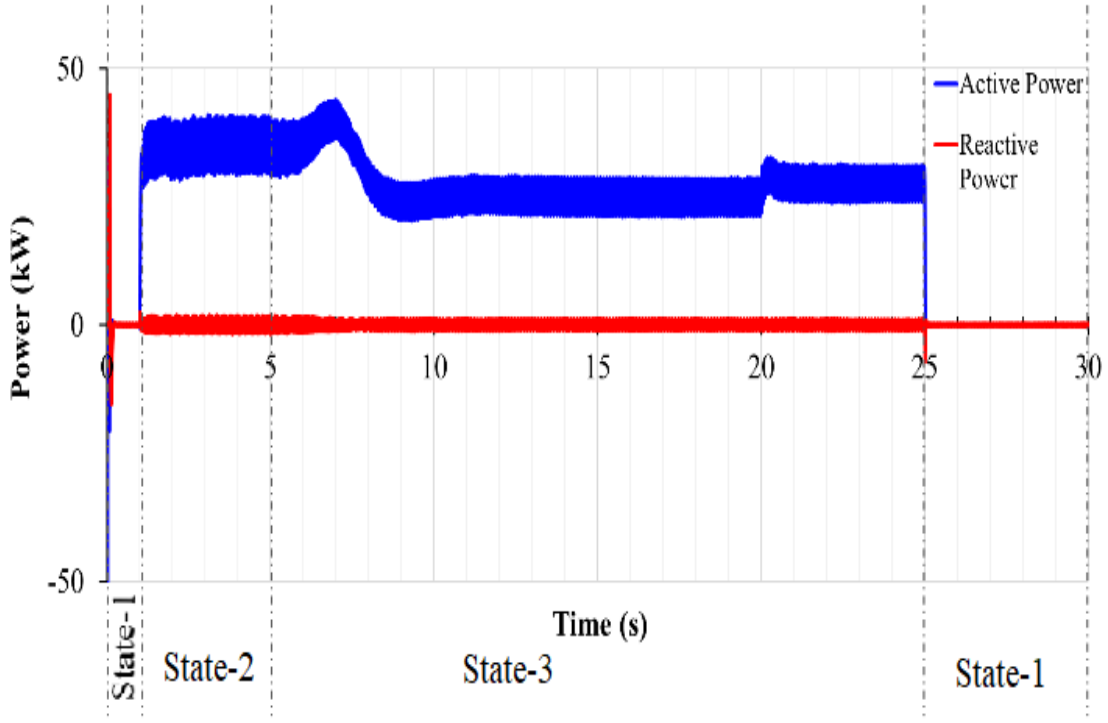


FIGURE 4.10: Active and Reactive Power Recorded at PCC During State-3 Operation.

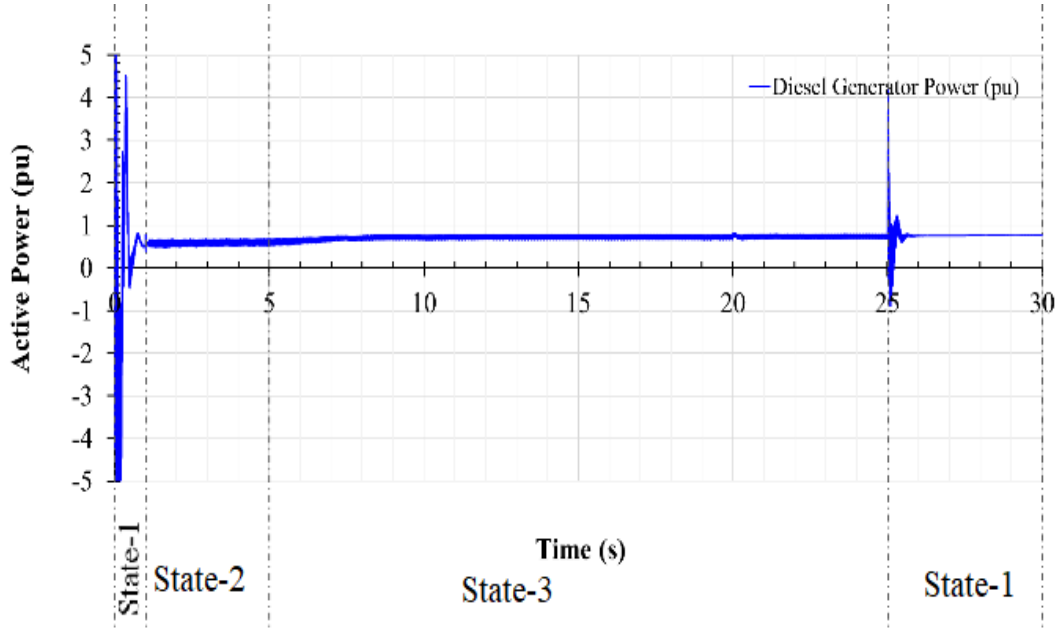


FIGURE 4.11: Output Active Power Supplied by Diesel Generator to the Utility Grid During State-3 Operation.

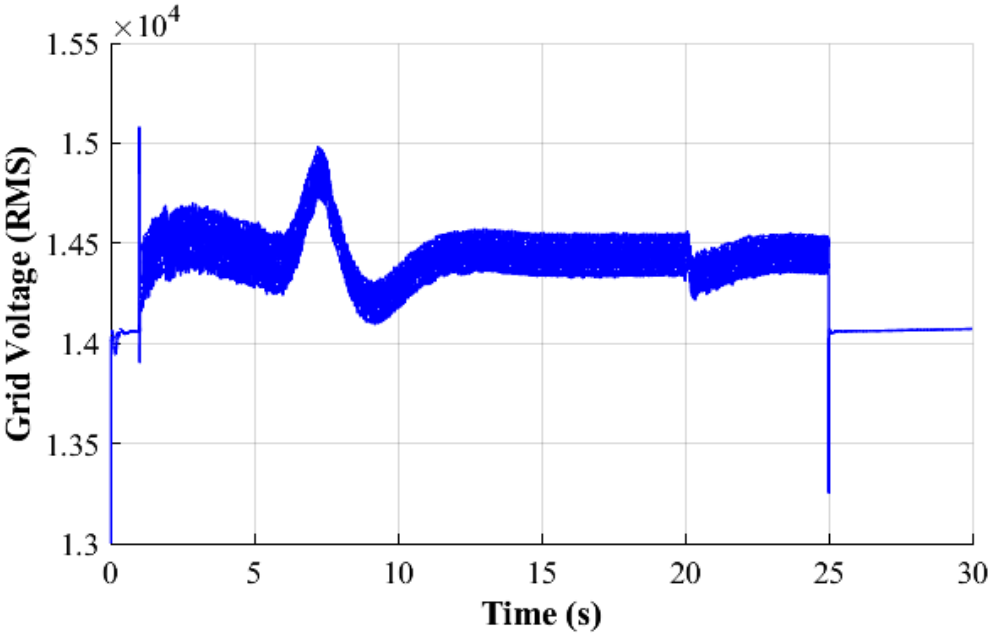


FIGURE 4.12: Phase-to-Neutral True RMS Grid Voltage During State-3 Operation.

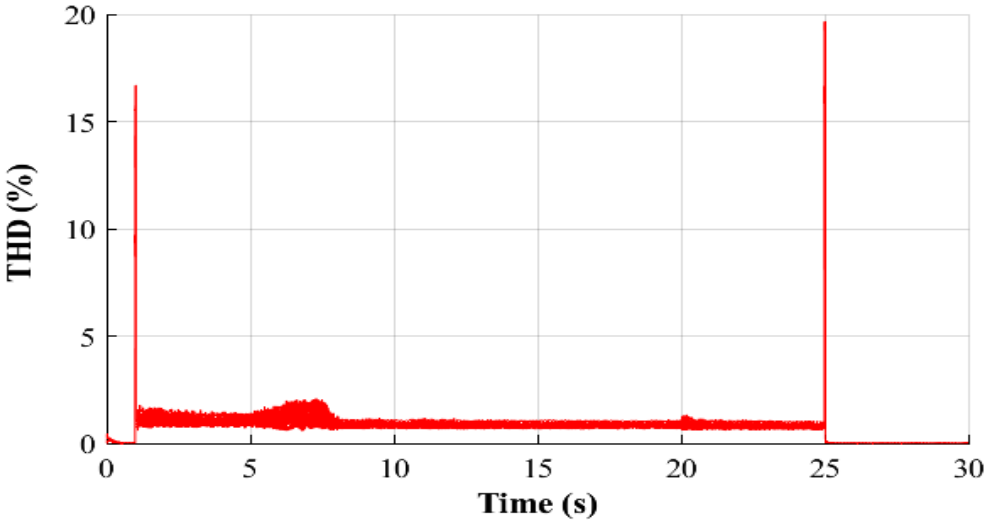


FIGURE 4.13: Total Harmonic Distortion in Phase-to-Neutral Grid Voltage During State-3 Operation.

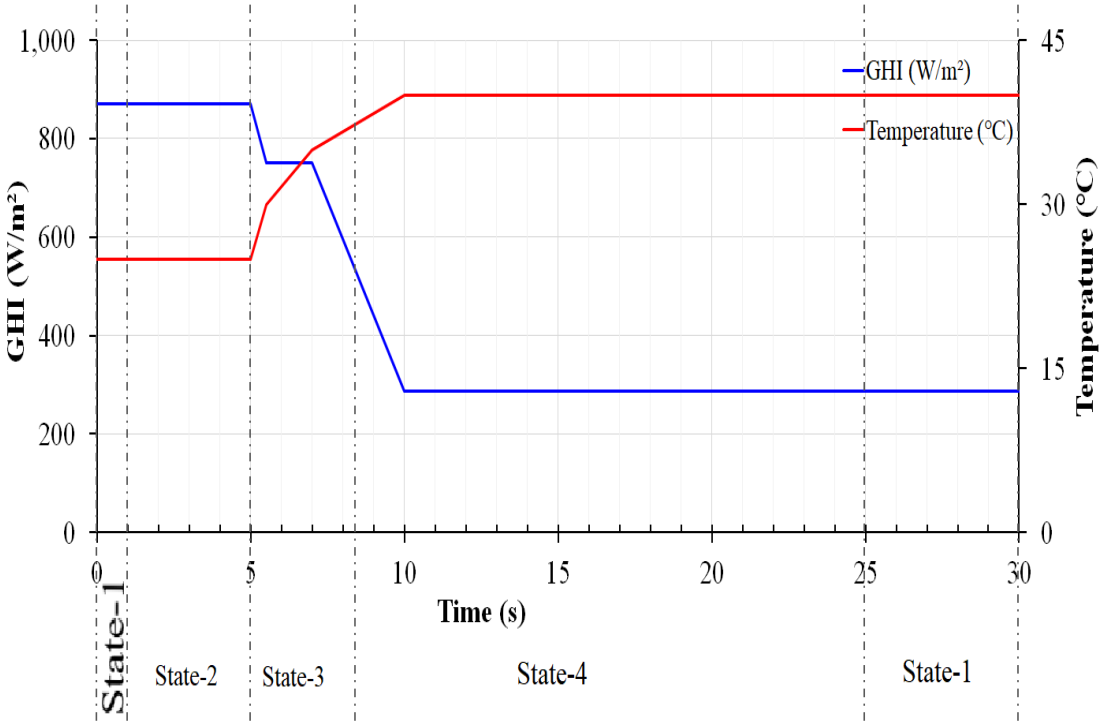


FIGURE 4.14: Simulated GHI and Temperature Profile in State-4 of Proposed EMS.

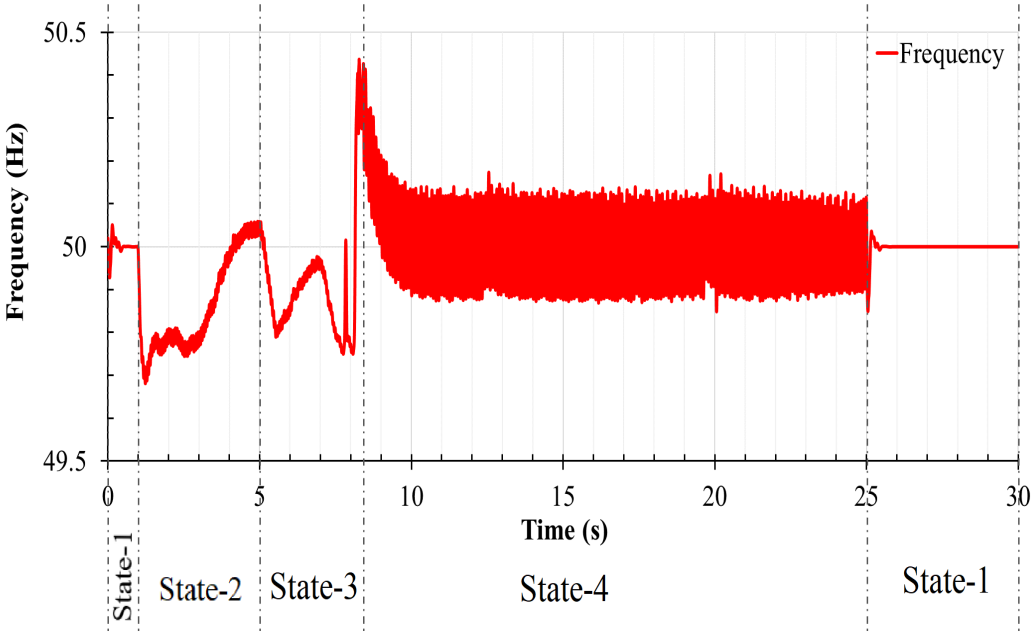


FIGURE 4.15: Grid Frequency Chart for State-4 Operation.

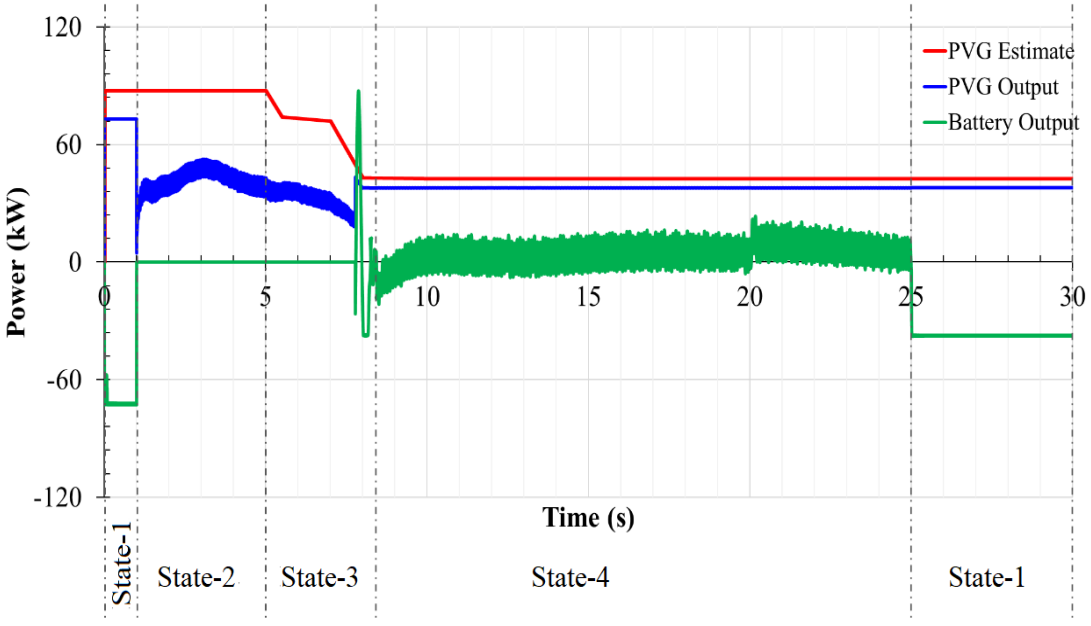


FIGURE 4.16: PVG's Forecasted and Aactual DC Power Output Level and BSS Output Power Level for State-4 Operation.

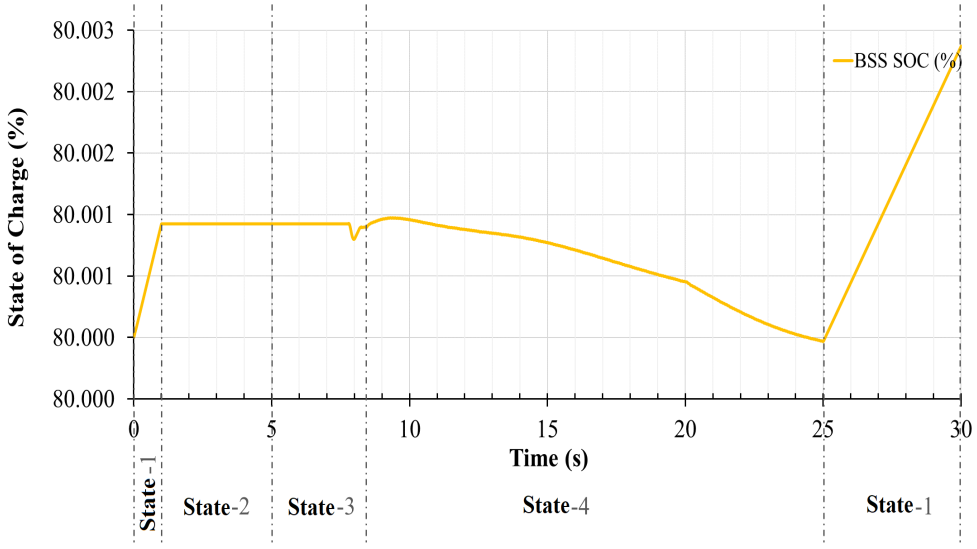


FIGURE 4.17: State of Charge (SOC) Level for BSS During State-4 Operation.

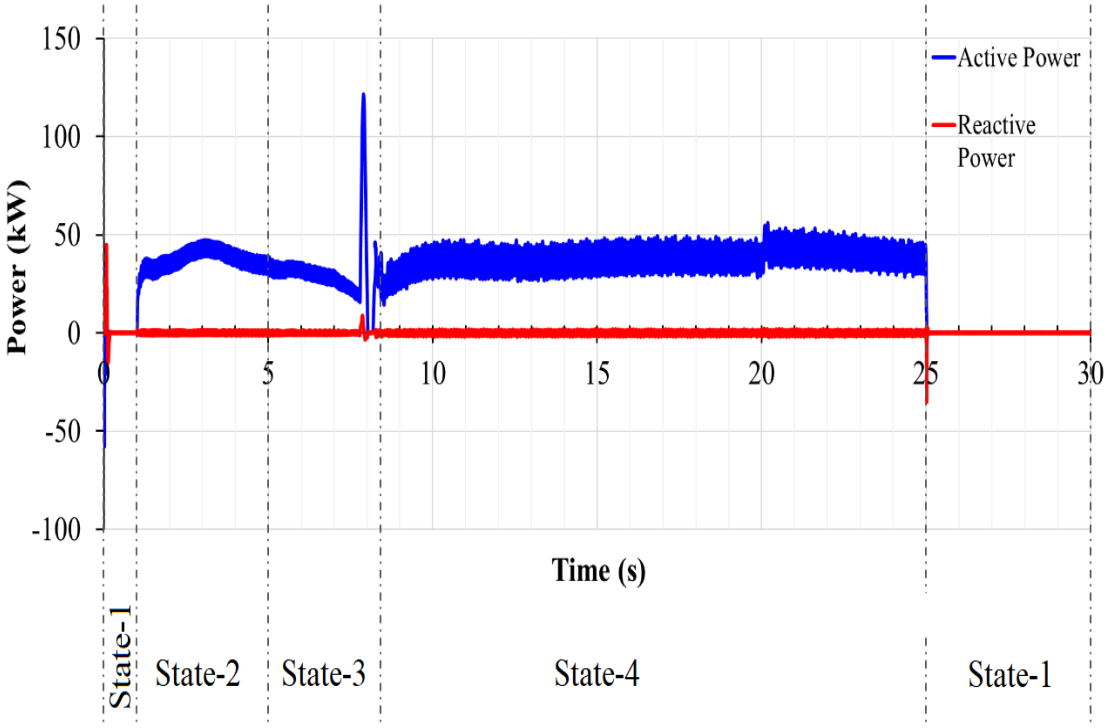


FIGURE 4.18: Output Active and Reactive Powers at PCC as Supplied by VSC to the Utility Grid.

Reason for zero reactive power (approximately) flow from VSC into grid as shown in figure 4.18 is due to sinusoidal waveform of grid-current as shonw in figure 4.20. After state-4 the grid voltage level is restored back to nominal 20kV RMS, as shown in figure 4.19.

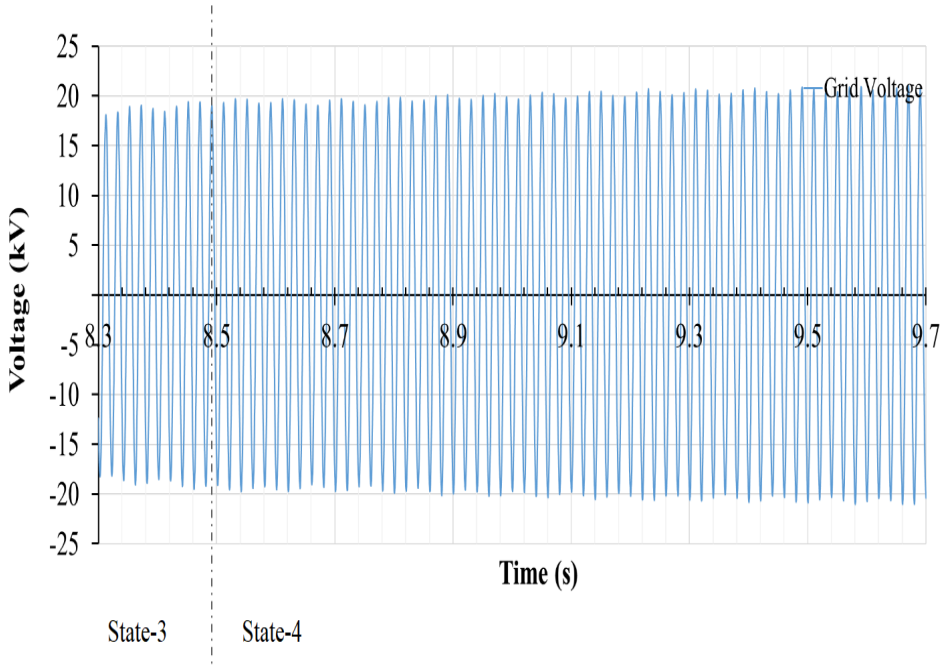


FIGURE 4.19: Instantaneous Phase-to-Neutral Grid Voltage, as Microgrid Transitions from State-3 into State-4.

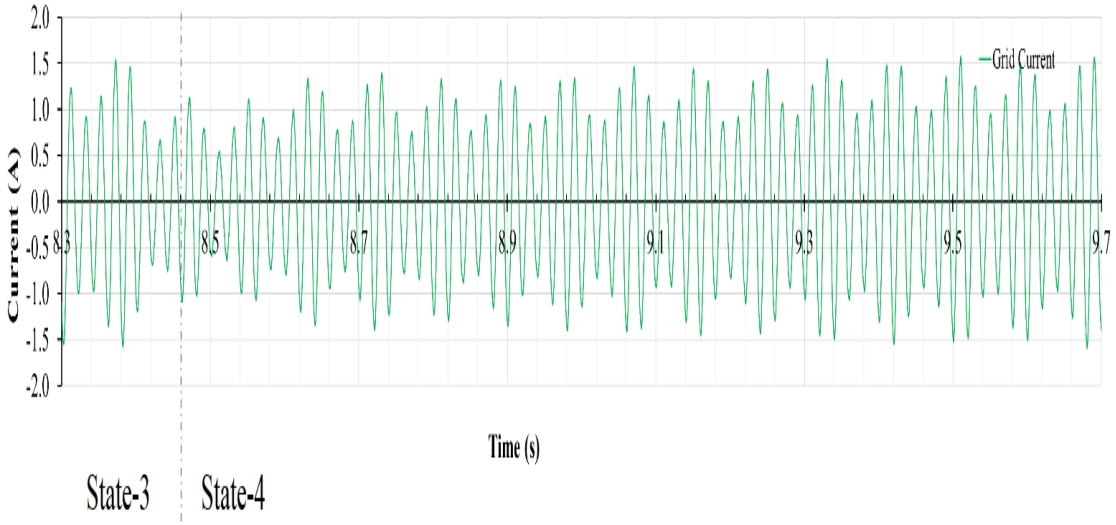


FIGURE 4.20: Instantaneous Grid Current, as Microgrid Transitions from State-3 into State-4.

Grid's true RMS voltage and THD levels are also EN-50160 compliant [74], as shown in figures 4.21 and 4.22 respectively. Inset in figure 4.21 displays a voltage dip before reentry in state-1. The dip lasts about 20ms and is categorized as swell, according to IEEE Std. 1159-2019 [73].

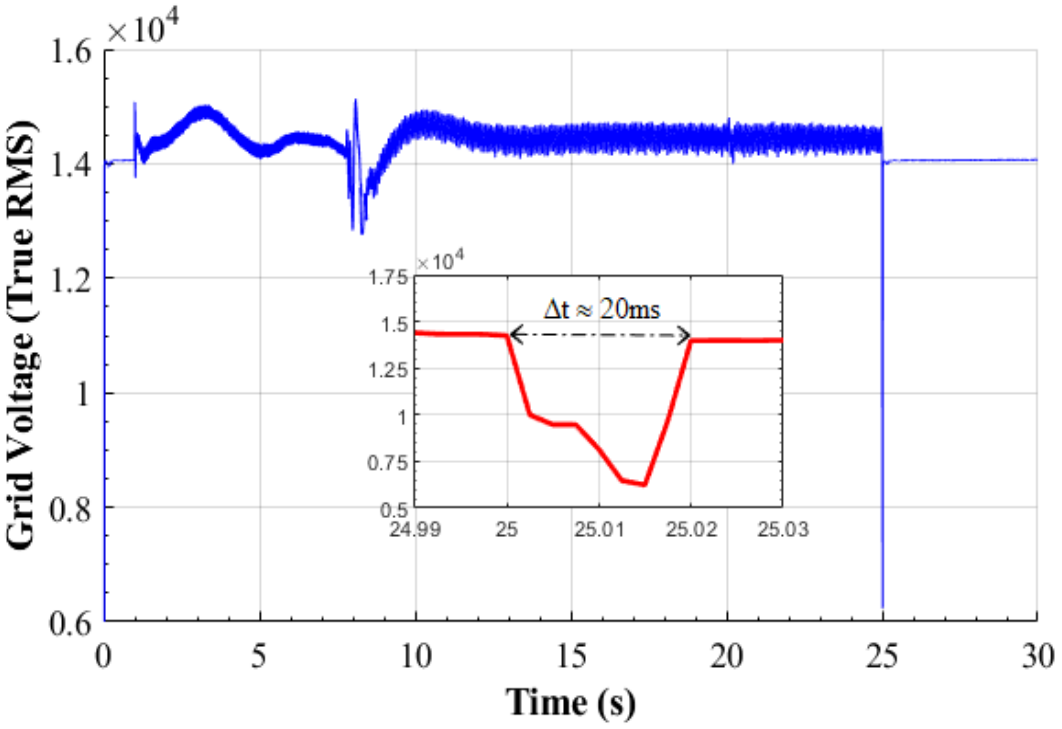


FIGURE 4.21: Phase-to-Neutral True RMS Grid Voltage During State-4 Operation.

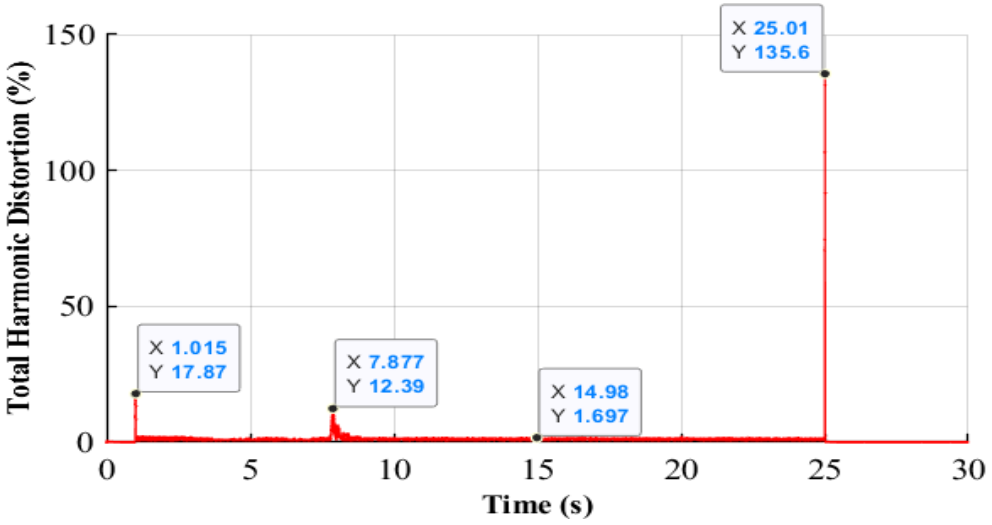


FIGURE 4.22: Total Harmonic Distortion in phase-to-Neutral Grid Voltage During State-4 Operation.

## 4.5 Summary

This chapter presented the application of PV power production forecast in the context of a sample hybrid microgrid. The major components of the sample microgrid are listed as a 100kW PV generator, 10kAh battery storage system, 75kW diesel generator, 75kW baseload, and 10kW auxiliary load. A multi-mode Energy Management Scheme (EMS) is proposed and operational details are outlined using a state diagram and a flowchart. Simulation results are presented for contingency events like source and load fluctuations. Transition between modes is presented using time-series charts and results are found within compliance limits set by standard EN-50160. It is concluded that an accurate PV output power forecast is crucial for stable hybrid microgrid operation.

# Chapter 5

# Conclusion and Future Work

## 5.1 Introduction

This chapter presents the conclusions drawn from this study, and a few recommendations for future work are also mentioned at the end.

## 5.2 Conclusion

This study presented a Machine Learning (ML) based Energy Management Scheme (EMS) for energy/power control of a hybrid microgrid. The ML model is selected from a pool of forecast models for a Photovoltaic Generator's (PVG) power output. The pool contained a deterministic model and three probabilistic models. A 100kW PVG benchmark model based on elementary loadline analysis is created for the sake of model/algorithm/technique qualification in Simulink®. Classical five-parameter solar cell model is used to formulate a deterministic (DTRM) prediction technique. DTRM model is a physical representation of PVG power output. DTRM model accepts global horizontal irradiance (GHI) and ambient temperature as inputs to forecast available maximum power output of the said PVG system. Probabilistic techniques are based on Machine Learning (ML) paradigm,

and a number of mainstream algorithms like Matern 5/2 Gaussian Process Regression (M5/2GPR), Rational Quadratic Gaussian Process Regression (RQGPR), and Support Vector Machine (SVM) are used. The GHI and temperature data of Islamabad, Pakistan is used for ML model training, validation, and testing. The performance of the entire pool of techniques is compared in terms of a quality index i.e., Root Mean Squared Error (RMSE). The most accurate technique or the one with the lowest RMSE is chosen and integrated in a proposed Energy Management Scheme (EMS).

Importance of an accurate forecast is validated by observing the EMS response during emergency events in a sample hybrid microgrid. The sample microgrid components are 100kW PVG, diesel generator, loads, and battery-based energy storage system. The proposed EMS distributes grid operation in four states, i.e., grid-connected state, islanding state, high-PV-islanded energy state, and low-PV-islanded energy state. The microgrid response is studied in the presence of several grid contingency events like source fluctuations and load fluctuations. The source fluctuations like GHI rise and fall are attributed to the non-uniform and non-stationary periodic rotational motion of Earth around the sun. The load fluctuations are due to uncertain consumption patterns of the electricity consumer. The grid imbalance is directly proportional to the grid frequency. Therefore, the grid frequency is considered an excellent grid health indicator; proposed EMS is completely based on regulation of grid frequency. The EMS continuously monitors the grid frequency and controls multiple energy sources at its disposal until the grid frequency is reverted back to its nominal value at 50Hz. Results in graphical charts validate optimized grid performance via compliance to the EN-50160 standard.

It is concluded that the non-linear and monotonic relationship between PV power output and input climate conditions is best described by a Gaussian Process Regression (GPR) model with Rational Quadratic (RQ) kernel function. Even though the prediction quality of RQ based GPR is very good, the training-time of DTRM and Linear Support Vector Machine (LSVM) are far better. Therefore, the RQ

based GPR model is deployed in the EMS and microgrid response is observed.

## 5.3 Future Work

A PV output power forecast technique is deployed in an EMS to manage energy components of a hybrid microgrid. EMS response is implemented and validated in a MATLAB® simulation. It is recommended that the proposed EMS must be validated using a hardware-in-the-loop (HIL) microgrid testbed like the one used in [74]. It is also desired that the EMS should be validated using instruments like multi-meters, Pyranometer and temperature transducers for real-time data acquisition and decision making. This work considered GHI and temperature as primary features for ML model training, validation and testing. However, a number of unmodeled dynamics like barometric pressure, diffuse horizontal irradiance, aging, partial shading, copper losses in interconnect wires, current leakage due to weak insulation etc., are potential ML features. Climate dataset can also be improved with advanced features like satellite imaging, cloud movement etc. Incorporation of these dynamics in future can lead to more accurate ML models, for round the year microgrid service.

# Appendix A

# Appendix

Table A.1: Physical Parameters of 100kW PV Generator.

| Parameters | Symbol | Value | Units |
|---|---|---|---|
| **Model Name** | - | SunPower Module (SPR-305E-WHT-D) | - |
| **No. of Cells** | $N_{CELL}$ | 96 | - |
| **No. of Series Modules** | $N_{SER}$ | 5 | - |
| **No. of Parallel Strings** | $N_{PAR}$ | 66 | - |
| **Maximum Power per module** | 305.226 | - | $W$ |
| **Maximum Power per array** | $P_{MPP}$ | 100.7 | $kW$ |
| **Short circuit current per module** | $I_{SC,n}$ | 5.9 | $A$ |
| **Temp. coefficient of $V_{OC}$** | $\beta_{voc}$ | -0.273 | $\%/^oC$ |
| **Open circuit voltage per module** | $V_{OC,n}$ | 64.2 | $V$ |
| **Temp. coefficient of $I_{SC}$** | $\alpha_{iSC}$ | 0.06175 | $\%/^oC$ |
| **Photocurrent** | $I_{PH,ref}$ | 6.01 | $A$ |
| **Reverse saturation current** | $I_{SAT,ref}$ | 6.3014 | $pA$ |
| **Ideality factor** | $n_i$ | 0.945 | - |
| **Parallel Resistance per module** | $R_{SH,ref}$ | 269.59 | Ohm |
| **Series Resistance per module** | $R_{SER,ref}$ | 0.375 | Ohm |
| **Nominal Irradiance** | $S_n$ | 1000 | $W/m^2$ |
| **Reference temperature** | $T_{Ref}$ | 298.15 | $K$ |
| **$\epsilon_g$ versus $T_{Cell}$ slope** | $d\epsilon_g/dT$ | -0.00027 | $eV/K$ |
| **Electron Charge** | $q$ | 1.603e-19 | $C$ |
| **Thermal voltage reference** | $V_{T,ref}$ | 2.331 | $V$ |

# Bibliography


[1] C. Wan, J. Zhao, Y. Song, Z. Xu, J. Lin, and Z. Hu, "Photovoltaic and solar power forecasting for smart grid energy management," *CSEE Journal of Power and Energy Systems*, vol. 1, no. 4, pp. 38–46, 2015.

[2] Z. Dong, D. Yang, T. Reindl, and W. M. Walsh, "Satellite image analysis and a hybrid ESSS/ANN model to forecast solar irradiance in the tropics," *Energy Conversion and Management*, vol. 79, pp. 66–73, 2014.

[3] S. Sumathi, L. A. Kumar, and P. Surekha, "Wind energy conversion systems," in *Solar PV and Wind Energy Conversion Systems*. Springer, 2015, pp. 247–307.

[4] E. M. Rodrigues, R. Melicio, V. Mendes, and J. P. Catalao, "Simulation of a solar cell considering single-diode equivalent circuit model," in *International conference on renewable energies and power quality, Spain*, 2011, pp. 13–15.

[5] ECEN2060 Introduction to power electronics course notes. [Accessed: November 24, 2019]. [Online]. Available: http//ecee.colorado.edu/ecen2060/matlab.html

[6] T. Esram and P. L. Chapman, "Comparison of photovoltaic array maximum power point tracking techniques," *IEEE Transactions on energy conversion*, vol. 22, no. 2, pp. 439–449, 2007.

[7] N. A. Kamarzaman and C. W. Tan, "A comprehensive review of maximum power point tracking algorithms for photovoltaic systems," *Renewable and Sustainable Energy Reviews*, vol. 37, pp. 585–598, 2014.

[8] What is Machine Learning? A definition. [Accessed: 15, December 2019]. [Online]. Available: https://expertsystem.com/machine-learning-definition

[9] J. R. Koza, F. H. Bennett, D. Andre, and M. A. Keane, "Automated design of both the topology and sizing of analog electrical circuits using genetic programming," in *Artificial Intelligence in Design'96*. Springer, 1996, pp. 151–170.

[10] C. M. Bishop, *Pattern recognition and machine learning*. Springer, 2006.

[11] Machine learning with MATLAB. [Accessed: December 15, 2019]. [Online]. Available: https://www.mathworks.com/campaigns/offers/machine-learning-with-matlab.html

[12] J. Antonanzas, N. Osorio, R. Escobar, R. Urraca, F. J. Martinez-de Pison, and F. Antonanzas-Torres, "Review of photovoltaic power forecasting," *Solar Energy*, vol. 136, pp. 78–111, 2016.

[13] M. Abdel-Nasser and K. Mahmoud, "Accurate photovoltaic power forecasting models using deep LSTM-RNN," *Neural Computing and Applications*, vol. 31, no. 7, pp. 2727–2740, 2019.

[14] H. Sheng, J. Xiao, Y. Cheng, Q. Ni, and S. Wang, "Short-term solar power forecasting based on weighted Gaussian process regression," *IEEE Transactions on Industrial Electronics*, vol. 65, no. 1, pp. 300–308, 2017.

[15] U. K. Das, K. S. Tey, M. Seyedmahmoudian, S. Mekhilef, M. Y. I. Idris, W. Van Deventer, B. Horan, and A. Stojcevski, "Forecasting of photovoltaic power generation and model optimization: A review," *Renewable and Sustainable Energy Reviews*, vol. 81, pp. 912–928, 2018.

[16] J. Liu, V. Vitelli, E. Zio, and R. Seraoui, "A novel dynamic-weighted probabilistic support vector regression-based ensemble for prognostics of time series data," *IEEE Transactions on Reliability*, vol. 64, no. 4, pp. 1203–1213, 2015.

[17] S. Han, Y.-h. Qiao, J. Yan, Y.-q. Liu, L. Li, and Z. Wang, "Mid-to-long term wind and photovoltaic power generation prediction based on copula function

and long short term memory network," *Applied Energy*, vol. 239, pp. 181–191, 2019.

[18] J. Wang, P. Li, R. Ran, Y. Che, and Y. Zhou, "A short-term photovoltaic power prediction model based on the gradient boost decision tree," *Applied Sciences*, vol. 8, no. 5, p. 689, 2018.

[19] C. Voyant, G. Notton, S. Kalogirou, M.-L. Nivet, C. Paoli, F. Motte, and A. Fouilloy, "Machine learning methods for solar radiation forecasting: A review," *Renewable Energy*, vol. 105, pp. 569–582, 2017.

[20] T. Sueyoshi and M. Goto, "Photovoltaic power stations in Germany and the United States: A comparative study by data envelopment analysis," *Energy Economics*, vol. 42, pp. 271–288, 2014.

[21] A. Mellit, M. Benghanem, and S. A. Kalogirou, "An adaptive wavelet-network model for forecasting daily total solar-radiation," *Applied Energy*, vol. 83, no. 7, pp. 705–722, 2006.

[22] A. U. Haque, M. H. Nehrir, and P. Mandal, "A hybrid intelligent model for deterministic and quantile regression approach for probabilistic wind power forecasting," *IEEE Transactions on power systems*, vol. 29, no. 4, pp. 1663–1672, 2014.

[23] C. B. Martinez-Anido, B. Botor, A. R. Florita, C. Draxl, S. Lu, H. F. Hamann, and B.-M. Hodge, "The value of day-ahead solar power forecasting improvement," *Solar Energy*, vol. 129, pp. 192–203, 2016.

[24] S.-G. Kim, J.-Y. Jung, and M. K. Sim, "A two-step approach to solar power generation prediction based on weather data using machine learning," *Sustainability*, vol. 11, no. 5, p. 1501, 2019.

[25] A. Rose, R. Stoner, and I. Pérez-Arriaga, "Prospects for grid-connected solar PV in Kenya: A systems approach," *Applied Energy*, vol. 161, pp. 583–590, 2016.

[26] H. Kanchev, D. Lu, F. Colas, V. Lazarov, and B. Francois, "Energy management and operational planning of a microgrid with a pv-based active generator for smart grid applications," *IEEE transactions on industrial electronics*, vol. 58, no. 10, pp. 4583–4592, 2011.

[27] M. G. De Giorgi, M. Malvoni, and P. M. Congedo, "Comparison of strategies for multi-step ahead photovoltaic power forecasting models based on hybrid group method of data handling networks and least square support vector machine," *Energy*, vol. 107, pp. 360–373, 2016.

[28] R. J. Bessa, A. Trindade, C. S. Silva, and V. Miranda, "Probabilistic solar power forecasting in smart grids using distributed information," *International Journal of Electrical Power & Energy Systems*, vol. 72, pp. 16–23, 2015.

[29] S. Al-Dahidi, O. Ayadi, M. Alrbai, and J. Adeeb, "Ensemble approach of optimized artificial neural networks for solar photovoltaic power prediction," *IEEE Access*, vol. 7, pp. 81 741–81 758, 2019.

[30] H. K. Elminir, Y. A. Azzam, and F. I. Younes, "Prediction of hourly and daily diffuse fraction using neural network, as compared to linear regression models," *Energy*, vol. 32, no. 8, pp. 1513–1523, 2007.

[31] S. Al-Dahidi, O. Ayadi, J. Adeeb, M. Alrbai, and B. R. Qawasmeh, "Extreme learning machines for solar photovoltaic power predictions," *Energies*, vol. 11, no. 10, p. 2725, 2018.

[32] J. Liu, W. Fang, X. Zhang, and C. Yang, "An improved photovoltaic power forecasting model with the assistance of aerosol index data," *IEEE Transactions on Sustainable Energy*, vol. 6, no. 2, pp. 434–442, 2015.

[33] E. Ogliari, A. Dolara, G. Manzolini, and S. Leva, "Physical and hybrid methods comparison for the day ahead pv output power forecast," *Renewable Energy*, vol. 113, pp. 11–21, 2017.

[34] X. Yan, D. Abbes, and B. Francois, "Uncertainty analysis for day ahead power reserve quantification in an urban microgrid including pv generators," *Renewable Energy*, vol. 106, pp. 288–297, 2017.

[35] P. Li, R. Dargaville, Y. Cao, D.-Y. Li, and J. Xia, "Storage aided system property enhancing and hybrid robust smoothing for large-scale PV systems," *IEEE Transactions on Smart Grid*, vol. 8, no. 6, pp. 2871–2879, 2016.

[36] J. Wang, R. Ran, and Y. Zhou, "A short-term photovoltaic power prediction model based on an FOS-ELM algorithm," *Applied Sciences*, vol. 7, no. 4, p. 423, 2017.

[37] L. Liu, Y. Zhao, D. Chang, J. Xie, Z. Ma, Q. Sun, H. Yin, and R. Wennersten, "Prediction of short-term PV power output and uncertainty analysis," *Applied Energy*, vol. 228, pp. 700–711, 2018.

[38] H. Esen, M. Esen, and O. Ozsolak, "Modelling and experimental performance analysis of solar-assisted ground source heat pump system," *Journal of Experimental & Theoretical Artificial Intelligence*, vol. 29, no. 1, pp. 1–17, 2017.

[39] P. Mathiesen, J. M. Brown, and J. Kleissl, "Geostrophic wind dependent probabilistic irradiance forecasts for coastal california," *IEEE Transactions on Sustainable Energy*, vol. 4, no. 2, pp. 510–518, 2012.

[40] S. Li, P. Wang, and L. Goel, "Wind power forecasting using neural network ensembles with feature selection," *IEEE Transactions on sustainable energy*, vol. 6, no. 4, pp. 1447–1456, 2015.

[41] M. B. Araújo and M. New, "Ensemble forecasting of species distributions," *Trends in ecology & evolution*, vol. 22, no. 1, pp. 42–47, 2007.

[42] O. M. Toledo, D. Oliveira Filho, and A. S. A. C. Diniz, "Distributed photovoltaic generation and energy storage systems: A review," *Renewable and Sustainable Energy Reviews*, vol. 14, no. 1, pp. 506–511, 2010.

[43] M. Alam, K. Muttaqi, and D. Sutanto, "Mitigation of rooftop solar pv impacts and evening peak support by managing available capacity of distributed

energy storage systems," *IEEE transactions on power systems*, vol. 28, no. 4, pp. 3874–3884, 2013.

[44] K. Agyenim-Boateng and R. Boehm, "Impact of storage integrated solar photovoltaics (PV) power system on utility peak loads," in *Energy Sustainability*, vol. 54686, 2011, pp. 1397–1406.

[45] M. Thomson and D. G. Infield, "Network power-flow analysis for a high penetration of distributed generation," *IEEE Transactions on Power Systems*, vol. 22, no. 3, pp. 1157–1162, 2007.

[46] R. Walling, R. Saint, R. C. Dugan, J. Burke, and L. A. Kojovic, "Summary of distributed resources impact on power delivery systems," *IEEE Transactions on power delivery*, vol. 23, no. 3, pp. 1636–1644, 2008.

[47] J. Hu, Y. Shan, Y. Xu, and J. M. Guerrero, "A coordinated control of hybrid ac/dc microgrids with PV-wind-battery under variable generation and load conditions," *International Journal of Electrical Power & Energy Systems*, vol. 104, pp. 583–592, 2019.

[48] Y. Xiang, J. Liu, and Y. Liu, "Robust energy management of microgrid with uncertain renewable generation and load," *IEEE Transactions on Smart Grid*, vol. 7, no. 2, pp. 1034–1043, 2015.

[49] M. Hosseinzadeh and F. R. Salmasi, "Robust optimal power management system for a hybrid AC/DC micro-grid," *IEEE Transactions on Sustainable Energy*, vol. 6, no. 3, pp. 675–687, 2015.

[50] Y. Zhang, N. Gatsis, and G. B. Giannakis, "Robust energy management for microgrids with high-penetration renewables," *IEEE transactions on sustainable energy*, vol. 4, no. 4, pp. 944–953, 2013.

[51] M. Afrasiabi, M. Mohammadi, M. Rastegar, and A. Kargarian, "Multi-agent microgrid energy management based on deep learning forecaster," *Energy*, vol. 186, p. 115873, 2019.

[52] M. Sechilariu, B. Wang, and F. Locment, "Building-integrated microgrid: Advanced local energy management for forthcoming smart power grid communication," *Energy and Buildings*, vol. 59, pp. 236–243, 2013.

[53] Pakistan - Solar radiation measurement data. [Accessed: December 31, 2019]. [Online]. Available: https://energydata.info/dataset/pakistan-solar-radiation-measurement-data

[54] G. Celsa and G. M. Tina, "MATLAB/Simulink model of photovoltaic modules/strings under uneven distribution of irradiance and temperature," in *IREC2015 The Sixth International Renewable Energy Congress*. IEEE, 2015, pp. 1–6.

[55] T. Ikegami, T. Maezono, F. Nakanishi, Y. Yamagata, and K. Ebihara, "Estimation of equivalent circuit parameters of pv module and its application to optimal operation of pv system," *Solar energy materials and solar cells*, vol. 67, no. 1-4, pp. 389–395, 2001.

[56] V. N. Vapnik, "The nature of statistical learning theory," *New York: Springer2V erlag*, 1995.

[57] K. Y. Bae, H. S. Jang, and D. K. Sung, "Hourly solar irradiance prediction based on support vector machine and its error analysis," *IEEE Transactions on Power Systems*, vol. 32, no. 2, pp. 935–945, 2016.

[58] C. E. Rasmussen and C. K. Williams, "Gaussian processes for machine learning the MIT press," *Cambridge, Mass*, 2006.

[59] R. M. Neal, "Priors for infinite networks," in *Bayesian Learning for Neural Networks*. Springer, 1996, pp. 29–53.

[60] Wikipedia., Islamabad. [Accessed: January 30, 2020]. [Online]. Available: https://en.m.wikipedia.org/wiki/islamabad

[61] Towards data science. [Accessed: January 2, 2020]. [Online]. Available: https://towardsdatascience.com/feature-selection-techniques-in-regression-model-26878fe0e24e

[62] I. Drouiche, S. Harrouni, and A. H. Arab, "A new approach for modelling the aging pv module upon experimental I-V curves by combining translation method and five-parameters model," *Electric Power Systems Research*, vol. 163, pp. 231–241, 2018.

[63] D. Wang, J. Qiu, L. Reedman, K. Meng, and L. L. Lai, "Two-stage energy management for networked microgrids with high renewable penetration," *Applied Energy*, vol. 226, pp. 39–48, 2018.

[64] X. Lu, K. Zhou, and S. Yang, "Multi-objective optimal dispatch of microgrid containing electric vehicles," *Journal of cleaner production*, vol. 165, pp. 1572–1581, 2017.

[65] S. Parhizi, A. Khodaei, and M. Shahidehpour, "Market-based versus price-based microgrid optimal scheduling," *IEEE Transactions on Smart Grid*, vol. 9, no. 2, pp. 615–623, 2016.

[66] E. Kuznetsova, Y.-F. Li, C. Ruiz, and E. Zio, "An integrated framework of agent-based modelling and robust optimization for microgrid energy management," *Applied Energy*, vol. 129, pp. 70–88, 2014.

[67] M. R. B. Khan, R. Jidin, and J. Pasupuleti, "Multi-agent based distributed control architecture for microgrid energy management and optimization," *Energy Conversion and Management*, vol. 112, pp. 288–307, 2016.

[68] M. Modiri-Delshad, S. H. A. Kaboli, E. Taslimi-Renani, and N. Abd Rahim, "Backtracking search algorithm for solving economic dispatch problems with valve-point effects and multiple fuel options," *Energy*, vol. 116, pp. 637–649, 2016.

[69] M. Zheng, C. J. Meinrenken, and K. S. Lackner, "Smart households: Dispatch strategies and economic analysis of distributed energy storage for residential peak shaving," *Applied Energy*, vol. 147, pp. 246–257, 2015.

[70] Grid levels. [Accessed: September 2, 2020]. [Online]. Available: https://www.swissgrid.ch/en/home/operation/power-grid/grid-levels.html

[71] T. Kerdphol, F. S. Rahman, Y. Mitani, M. Watanabe, and S. Küfeoğlu, "Robust virtual inertia control of an islanded microgrid considering high penetration of renewable energy," *IEEE Access*, vol. 6, pp. 625–636, 2017.

[72] Voltage disturbances standard EN 50160 - Voltage characteristics in public distribution systems. [Accessed: December 1, 2019]. [Online]. Available: http://copperalliance.org.uk/uploads/2018/03/542-standard-en-50160-voltage-characteristics-in.pdf

[73] 1159-2019 - IEEE recommended practice for monitoring electric power quality. [Accessed: July 14, 2020]. [Online]. Available: https://ieeexplore.ieee.org/servlet/opac?punumber=8796484

[74] B. Xiao, M. Starke, G. Liu, B. Ollis, P. Irminger, A. Dimitrovski, K. Prabakar, K. Dowling, and Y. Xu, "Development of hardware-in-the-loop microgrid testbed," in *2015 IEEE energy conversion congress and exposition (ECCE)*. IEEE, 2015, pp. 1196–1202.